Finescale Radar Observations of the Dimmitt, Texas (2 June 1995), Tornado

Joshua Wurman

School of Meteorology, University of Oklahoma, Norman, Oklahoma

Swarndeep Gill

Department of Atmospheric Sciences, University of Wyoming, Laramie, Wyoming

ABSTRACT

The mature and dissipating stages of a strong tornado were observed from close range by the prototype Doppler On Wheels mobile radar. Volumetric observations repeated eight times over an 840-s period with resolution volumes at the center of the tornado as low as 61 m $\times$ 61 m $\times$ 75 m = 2.8 $\times$ 10⁵ m³ revealed new details about three-dimensional tornado vortex structure and evolution. Observed structures included a conical debris envelope, a low-reflectivity eye, multiple windfield maxima, and multiple semiconcentric bands of reflectivity surrounding the eye. The three-dimensional structure of the debris and single-Doppler wind field were well characterized, as well as more rapid dissipation of the tornado aloft compared to near the ground. Volumetric measures of tornado strength are introduced. A downdraft exhibiting $w \sim -30$ m s⁻¹, indicative of a partial two-cell vortex, was observed only during the earliest radar scans when the tornado was near maximum intensity. Comparisons with simple conceptual models of vortices are presented and asymmetries are described. Possible reasons for the lack of radar-observed surface convergence are discussed. Comparisons between observed winds and damage are presented and a potential Fujita scale is introduced.

1. Introduction

Numerous studies of tornadoes and tornadic storms have employed computer models (Rotunno 1977, 1979, 1984, 1986; Lewellen et al. 1997), radar observations (Fujita 1958; Wakimoto et al. 1996, 1998; Wakimoto and Atkins 1996; Wakimoto and Martner 1992; Bluestein et al. 1993, 1995; Brown et al. 1978; Brandes 1984; Johnson et al. 1987; Zrnic et al. 1985; Smith and Holmes 1961; Zrnic and Doviak 1975; Burgess and Lemon 1990), conceptual models (Lewellen 1993; Davies-Jones 1986), or laboratory simulations (Ward 1972; Davies-Jones 1973; Church and Snow 1993; Church et al. 1979). Until recently, however, *high-resolution three-dimensional* observations of tornado vortices themselves, particularly in the optically inaccessible interior, have been nonexistent. Therefore, computer and conceptual model predictions have remained largely unverified. Most radar studies of tornadoes have been limited by the typical range of tornadoes to stationary radars, resulting in beam spreading and beam departure from the earth's surface. This severely limits the ability to resolve tornado-scale structures (Wurman et al. 1997;

Corresponding author address: Dr. Joshua Wurman, University of Oklahoma, 100 E. Boyd, Norman, OK 73019.
E-mail: jwurman@ou.edu

Burgess et al. 1993; Wood and Brown 1997). Notable high-resolution observations of tornadoes and tornadic storms include Bluestein et al. (1993) and Bluestein et al. (1995) who described observations of a tornado and a severe thunderstorm with mobile 30- and 3-mm wavelength radar systems, respectively, and Wakimoto and Martner (1992) who described observations of a nonsupercell-spawned tornado from 12-km range. Wakimoto et al. (1998) described pseudo-dual-Doppler observations of a tornadic storm retrieved from the Electra Doppler Radar (ELDORA) airborne Doppler radar (Hildebrand and Mueller 1985) from a range of 12 km.

The prototype Doppler On Wheels (DOW) radar (Wurman et al. 1997) was developed for the purpose of obtaining high-resolution observations of tornadoes and other short-lived and small-scale atmospheric phenomena. This DOW could deploy and undeploy quickly in severe weather environments, conduct volumetric scans at rapid update rates, and display Doppler velocity and reflectivity data in real time for coordination and safety purposes. The DOW was first employed in the final weeks of the Verification of the Origin of Rotation in Tornadoes Experiment (VORTEX) (Rasmussen et al. 1994). It collected data in several tornadoes (Wurman et al. 1996) from ranges of less than 3 to over 20 km, resulting in radar resolution volumes as small as 40 m $\times$ 40 m $\times$ 75 m. Observations of one of these tornadoes,
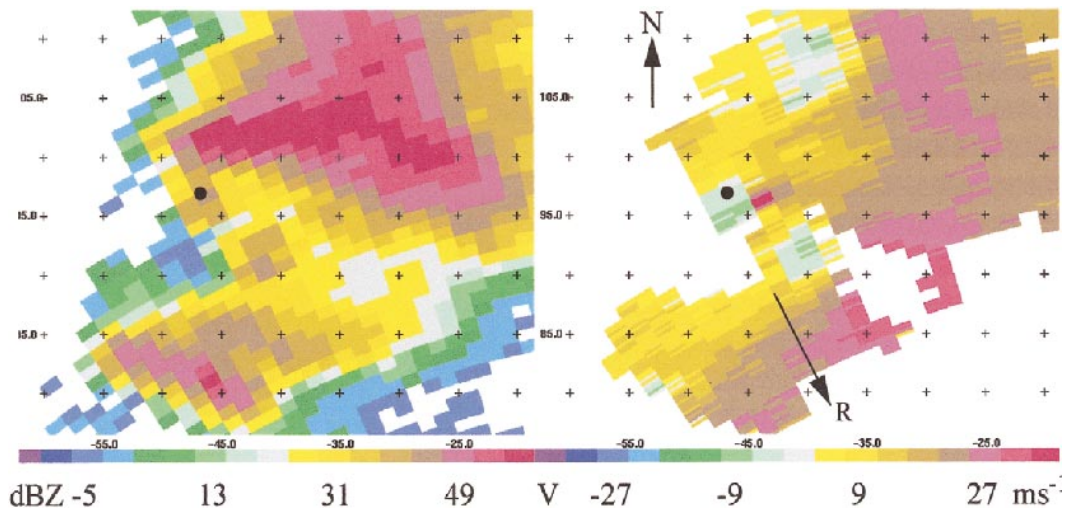
FIG. 1. Tornadic thunderstorm near Dimmitt, TX, as viewed from the Lubbock, TX, radar. Data were from the KLBB WSR-88D at 0102 UTC 0.5° elevation angle. (left) Radar reflectivity showing a supercellular thunderstorm with hook echo well defined by the 40-dBZ contour. (right) Doppler velocity showing a velocity couplet ΔV, approximately 45 m s^{-1}, associated with the tornado. The location of the deployed DOW radar is indicated in each panel with black dots. Tick marks define a 5-km grid. At the 107-km range of the DOW, KLBB radar beams were approximately 1 km AGL and the beamwidths were approximately 2 km, preventing resolution of the tornado itself. Arrow marked ''R'' indicates direction of radar.

observed at close range for 960 s, with resolutions ranging from 61 m $\times$ 61 m $\times$ 75 m = 2.8 $\times$ 10^5 m^3 to 94 m $\times$ 94 m $\times$ 75 m = 6.7 $\times$ 10^5 m^3, are presented here.

2. Radar, site, and data description

a. DOW radar description

The prototype DOW was described in detail in Wurman et al. (1997). It was a 32-mm wavelength (9.375 GHz or X band) magnetron radar that used a surplus transmitter from the National Center for Atmospheric Research's (NCAR) CP-2 radar (Keeler et al. 1989). The transmitter was nominally capable of transmitting 0.5-μs pulses at 40-kW peak power. It is likely that the true peak power was 0.3–1.0 of this value during 1995. The pulse repetition time was 0.5 ms. The antenna was 1.83 m in diameter resulting in a 1.2° beamwidth. About a week before the Dimmitt tornado, the feedhorn hit a tree branch and had to be realigned visually. Subsequent testing revealed that the beam was restored to proper alignment with acceptable, but not quantitatively measured, sidelobe levels. Signal processing was conducted on an NCAR PC Integrated Acquisition processor (PIRAQ) (Wurman et al. 1997). Data sampling matched the pulsewidth at 0.5 μs, resulting in a spatial resolution of 75 m in the radial direction.

The prototype DOW radar was created in less than six months and rushed into service for the last three weeks of VORTEX in 1995. While capable of retrieving high-resolution Doppler radar data, it was immature, largely untested, and thus only partially functional and incomplete in many respects. The leveling system was crude and only accurate to within about 0.5°. There was

no navigational or spatial orientation equipment, so radar location and orientation had to be inferred post facto as described below. Transmitted power, system losses, and receiver noise levels and gain were not well characterized, so radar reflectivity levels were uncalibrated and approximate, subject to an uncertainty of at least ±3 dB. System time was also only crudely calibrated with UTC, with resultant uncertainties as discussed in section 3a. It was believed that this system time was 120 s behind UTC, but this could not be confirmed directly with the data presented herein or by comparing with time-tagged visual observations from VORTEX crews. Due to computer difficulties, up to 70% of all data beams might have been dropped and not recorded.

b. Deployment site description and navigation of data

On 3 June 1995 at 0100 UTC (2000 CDT 02 June 1995) a supercell thunderstorm was moving northeastward through the Texas Panhandle. The Lubbock, Texas, Weather Surveillance Radar-1988 Doppler (WSR-88D) (KLBB) was able to observe the storm from 107-km range (Fig. 1). Just after 0100 UTC, a tornado was reported by VORTEX crews. The DOW deployed to the south of the town center (Fig. 2), approximately 3 km north of the tornado. The site was surrounded by farm fields in the southern and eastern directions, but trees, a house, and other structures to the northeast (visible in Fig. 3) blocked radar beams below about 2° elevation. The DOW began observations at 0103 UTC, by which time the tornado had moved slowly northeastward and was 3 km to the southeast of the site. The tornado was
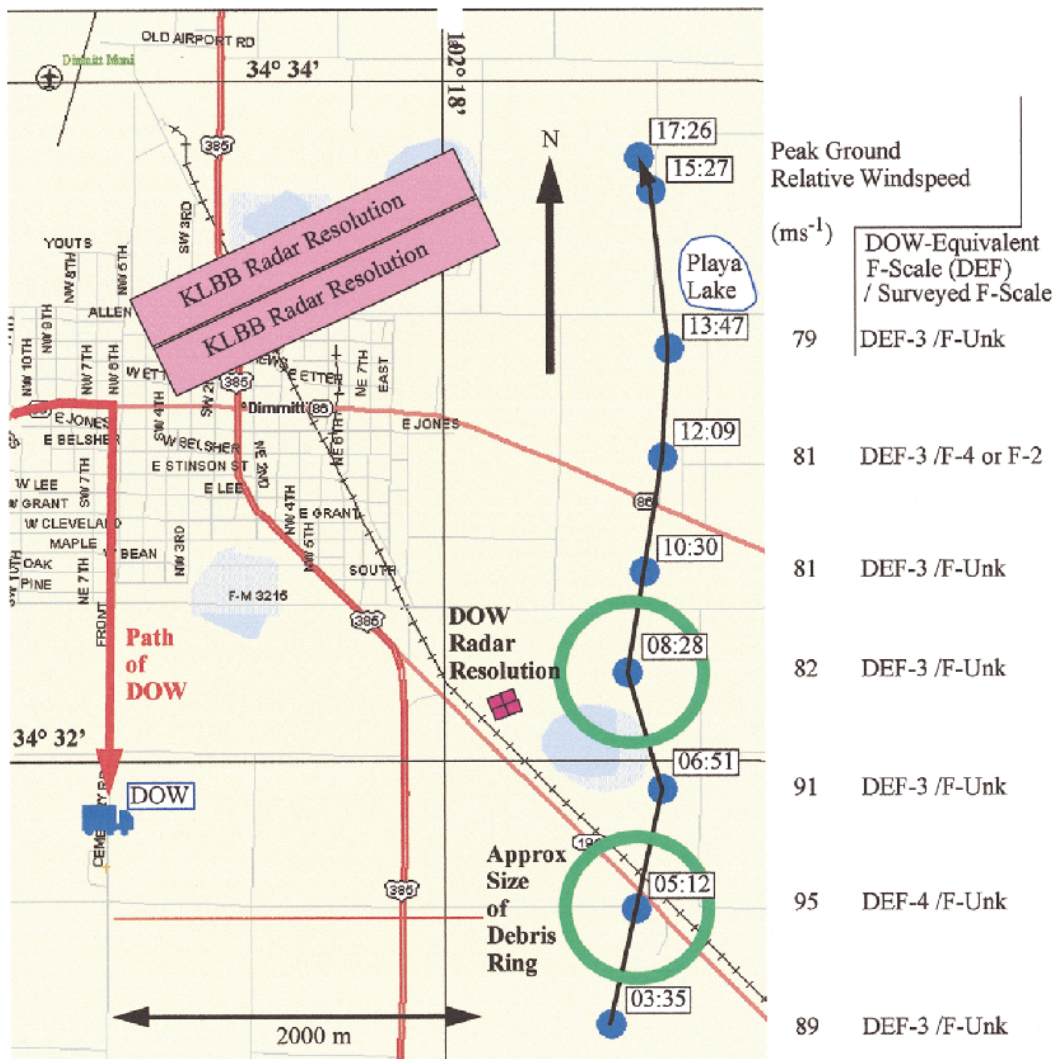
FIG. 2. Track of the Dimmitt tornado with deployment path and location of DOW mobile radar just after 0100 UTC 3 Jun 1995. Track represents location of near-surface circulation of tornado with times plotted in mm:ss after 0100 UTC. The uncertainty in locations are approximately 50 m, slightly smaller than the size of the plotted blue circles. Peak DOW-indicated ground-relative wind speeds adjusted for observation aspect ratio as well as the PF scale and surveyed F-scale ratings are listed to the side of the track. KLBB radar (Lubbock, TX, 107 km away) and DOW resolution areas are illustrated with pink rectangles. The approximate diameter of the debris ring during the first five volume scans is shown by two representative green circles.

visually characterized by a large condensation funnel extending to the ground and a pronounced debris cloud at the earliest observation times (Fig. 3, top). It became narrower with less surrounding debris, then ropelike and only visible well above the ground prior to dissipation to the northeast of the town center several minutes later (Fig. 3, bottom left and right).

In order to determine the precise location and orientation of the DOW, post facto, which should help with future comparisons among DOW, airborne radar, and damage survey data, two independent methods were used. During the data collection period, several photographs of the DOW and the surrounding site were taken. In these photographs, several structures, includ-

ing a nearby house and the Goodpasture fertilizer plant were visible. Two years later one of the authors (SG), equipped with these photographs and a Global Positioning System (GPS) receiver, surveyed the site. The structures visible in the photographs provided multiple points of visual comparison and permitted determination of the DOW location to a precision of 50 m, less then the radar resolution volume at the range of the tornado. Since the site was known to be within 10 m of a particular north–south-oriented road, the only free parameter in this process was the location along this road. GPS readings were repeated at this site several times over a several-hour period in order to determine the latitude and longitude within 50 m.

FIG. 3. (top) DOW radar with the Dimmitt tornado in the background at approximately 0107 UTC. The view is approximately to the east. The debris cloud is clearly visible. The southern edge of the condensation funnel is barely visible above "A." The center of the tornado (not visible due to dust and condensation) is approximately 3000 m away. The visible edge is approximately 2500 m away. (bottom left) View to northeast of weakening tornado. Narrow condensation funnel is visible through more diffuse debris cloud. (bottom right) Rope-stage dissipation of tornado at approximately 0117 UTC. The tornado may extend to the ground, invisibly, at this time, possibly accounting for the discrepancy between DOW-indicated locations and VORTEX team visually indicated locations. The tornado is approximately 5000 m away. Photograph times were not recorded; times are estimated from location and photograph sequence.

The location and orientation of the DOW was determined independently by comparing clutter echo features that appeared in the lowest radar scans to a detailed road map of the area. Clutter echoes were most likely caused by electrical and telephone lines immediately adjacent to roads. A typical clutter map and annotated road map are illustrated in Fig. 4. Several comparison features are illustrated. Using this method, the uncertainty in the estimated location of the DOW was within the length of a radar resolution volume, 75 m, and the error in the

$\rightarrow$

FIG. 4. Annotated clutter map and street map in the vicinity of Dimmitt. Key points of comparison are shown in both maps. These and other comparisons were used to precisely define the DOW orientation correction of 99.8°. Due to a ranging offset in the DOW data, the virtual location of the DOW radar was approximately 220 m behind the actual radar, as indicated by the black circle. Labelled range rings are at intervals of 1 km.
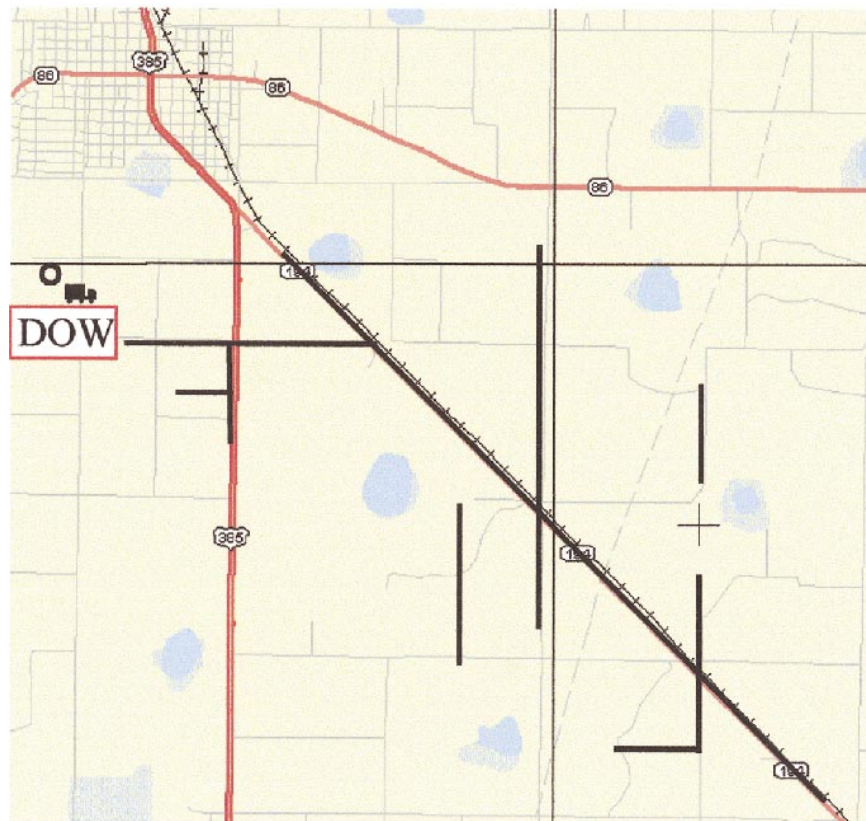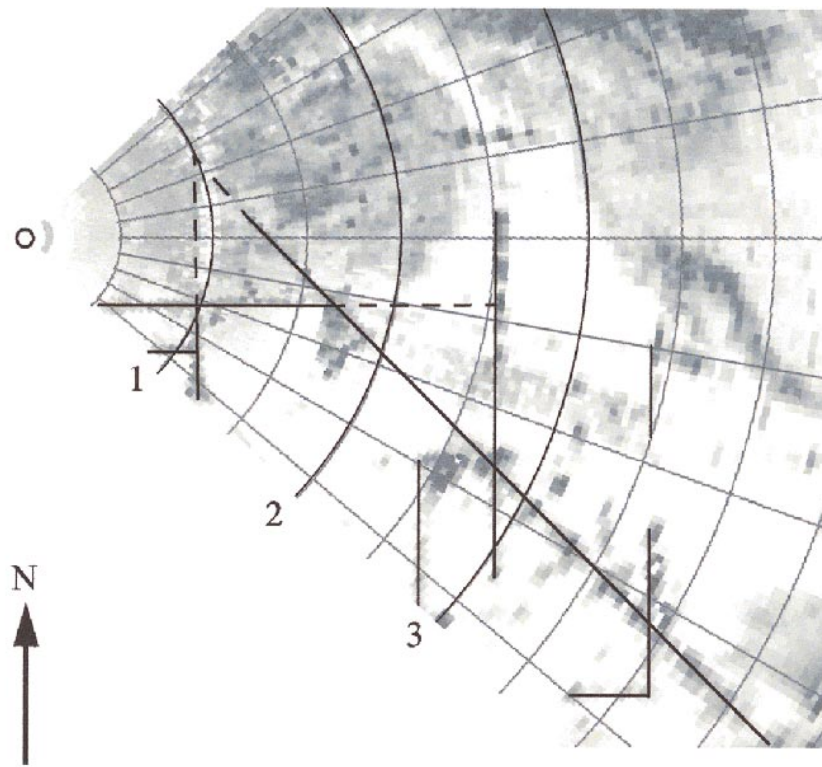
orientation of the DOW was $\pm1.0°$, which was less than the radar beamwidth, resulting in a location error of ±52 m at a range of 3 km. (A 220-m-range offset in the data, caused during data translation, was subtracted. When the antenna was pointing forward relative to the truck, DOW data indicated an azimuth of 132°.) To within 50 m, the DOW was determined to be located at $34°31.82 \pm 0.03'$N and $102°19.20 \pm 0.03'$W with 0° DOW-indicated azimuth equal to $99.8° \pm 1.0°$ true azimuth, measured clockwise from north.

c. Data collection strategy and data processing

As the DOW was being leveled, partial volume sector scans were initiated. Scanning was conducted through azimuthal sectors of approximately 90°, at 10 stepped elevation angles of 0°, 1°, 2°, 4°, 6°, 8°, 10°, 12°, 14°, and 18°. Antenna control software and hardware were relatively crude, so elevation angles were not constant through each sector sweep, particularly through the first 20° of azimuth in each sweep. The scanning rate of the antenna was $10° \text{ s}^{-1}$, resulting in scan repetition intervals of 100 s. Velocity and reflectivity data were processed using standard pulse-pair methods, integrating over 64 pulses. With a pulse repetition time of 0.5 ms, this would have resulted in approximately 30 beams per second, or two beams per degree of azimuth, oversampling the 1.2° radar beamwidth by approximately a factor of 2–3. Unfortunately, computer system limitations resulted in 30%–70% of beams being dropped, resulting in approximately one or two beams per azimuthal degree, at least matching the radar beamwidth. The scales of motion well resolved by the DOW were a few to several times greater than the DOW resolution volumes (Carbone et al. 1985). Certainly features below 100–200 m in scale were not well resolved. Data collection commenced near the end of an volumetric scan at 0102:45 UTC and eight complete sets of sector scans through the tornado were collected from 0103:26 through 0116:56 UTC, then an incomplete volume scan was collected, after which the tornado dissipated.

Data were processed and stored in a field format that could be translated into conventional radar quantities such as Doppler velocity, received power, equivalent radar reflectivity factor, normalized coherent power (NCP), and other derived quantities. Translation into NCAR DORADE format, display, and editing were accomplished using the NCAR SOLO software suite, Xltrs, Solo, Reorder, and Zebra.

With a pulse repetition period of 0.5 ms and a wavelength of 32 mm, the data exhibited a Nyquist interval of 32 m s^{-1} (Doviak and Zrnic 1993) resulting in velocity aliasing at ±16, ±48, and $\pm80 \text{ m s}^{-1}$. Data were manually dealiased by adding or subtracting multiples of 32 m s^{-1} to the affected data regions (Fig. 5). This was a subjective process, but the choice to add or subtract 32 m s^{-1} was usually quite clear cut. The extremely high resolution of the DOW data, significantly smaller than the tornado core radius, resulted in gate-to-gate shears of much less than the Nyquist interval in almost all regions. Vertical and temporal continuity provided further buttressing of dealiasing choices. As in any subjective procedure, however, it was possible that outlying, but valid, data were eliminated, or rather dealiased, into conformity with presupposed notions of tornado vortex structure. Further confirmation of the implied conceptual models inherent in these subjective choices was obtained by referring to even higher resolution data retrieved in two tornadoes in 1998, at resolutions of 20 m × 20 m × 38 m and 3 m × 3 m × 38 m. Data presented here were manually filtered to eliminate areas of severe ground clutter contamination. The data were also filtered to eliminate velocity values associated with NCP values of less than 0.15 (Fig. 5d). In regions with very low NCP values, low received power and/or extreme turbulence precluded the accurate determination of Doppler velocities. This occurred frequently in the low-reflectivity eye of the tornado and sometimes in the core flow region where velocities and shears were highest. These excluded data are indicated with pink/lavender in all velocity images.

3. Description of the tornado

a. Track

Since the data from the 0° elevation radar sweeps were severely contaminated by ground clutter, it was difficult to determine accurately the center of the tornado at the lowest observed levels. Data from the 1° elevation sweeps were used instead. At the earliest radar observation times, the tornado was at 3-km range, approaching 2.9 km, then moving away to 4.5–5-km range at dissipation. Thus, the 1° scans represented data centered 51 m to 87 m above ground level (AGL). Barring tornado inclinations in excess of 45°, the center locations determined using these 1° sweeps were within about one radar resolution area (61 × 75 m at 2.9 km, 94 × 75 m at 4.5 km) of the location of the tornado at the surface. The tornado center was determined from both the radar reflectivity and Doppler velocity data. Velocity and reflectivity determined centers usually agreed to within one radar resolution area. Table 1 contains the azimuth and range and latitude–longitude of the tornado at the time of each 1° scan; the track is illustrated in Fig. 2.

While the early portion of the radar determined track agreed well, geographically, with a track determined from preliminary VORTEX crew visual observations, the times at which the tornado was at specific locations along the track as indicated by DOW data and VORTEX visual observations disagreed by varying amounts ranging from 20 to 150 s. The possibility of short period drift in the DOW system clock was explored and discounted. During the three years following these observations, including hundreds of independent time calibrations, no time drifts relative to GPS indicated UTC
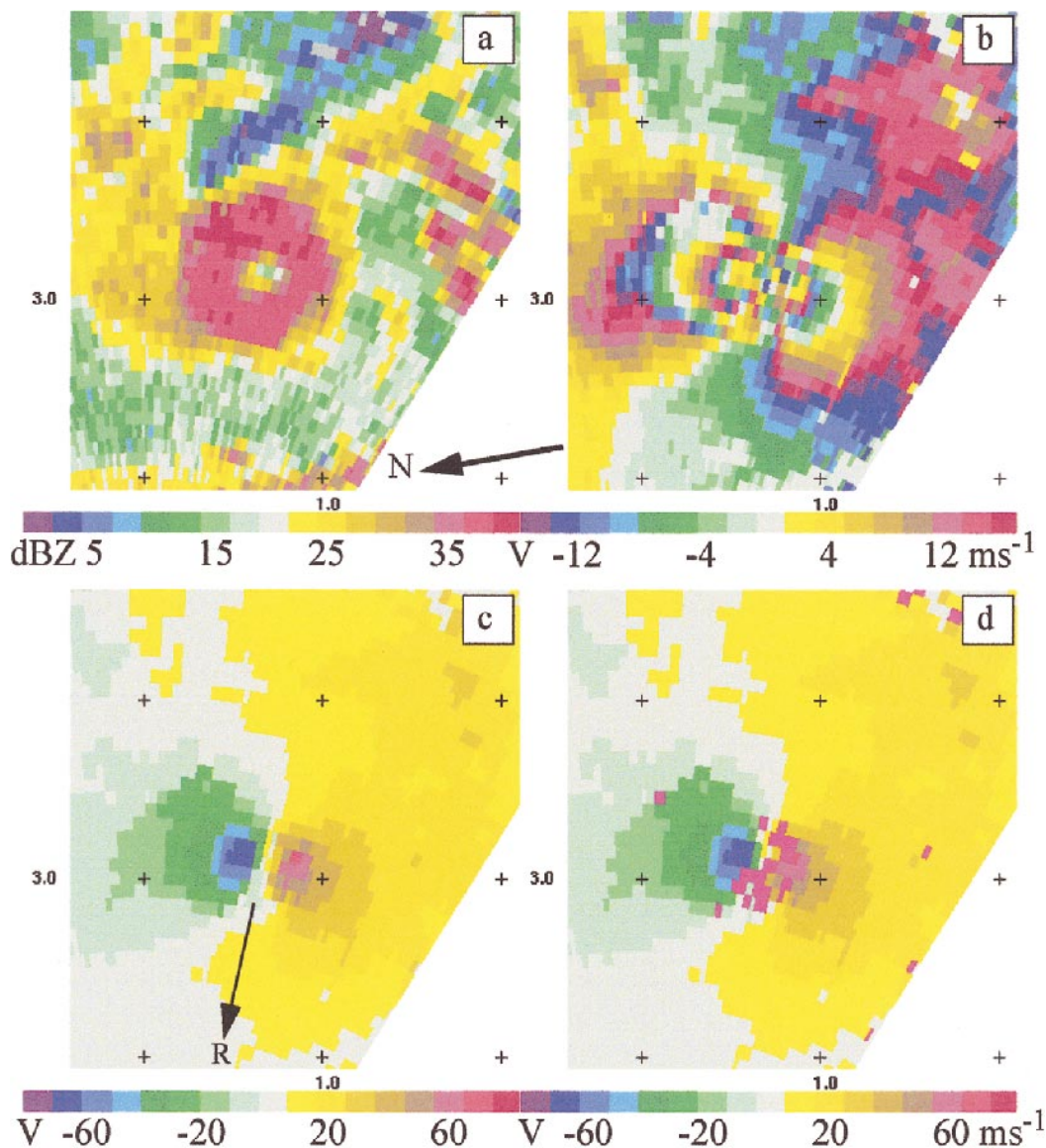
FIG. 5. Illustration of velocity data processing. Panels show data in and near tornado. (a) Uncalibrated radar reflectivity. (b) Raw Doppler velocity with incorrect sign. (c) Subjectively dealiased Doppler velocity. (d) Final Doppler velocity after filtering for ground clutter and for regions with low normalized coherent power. Data that has been filtered out is indicated as bright pink/lavender in this and all other figures. All data from 1.0° scan at 0103:35 UTC. Height of radar beam at tornado center was about 60 m AGL. As in all horizontal-slice radar images, except Figs. 1, 15, and 24, tick marks define 1-km grid. Reflectivity scale in dBZ. Velocity scale in m s^{-1}. The arrow labeled "R" in (c) indicates the direction to the DOW.

exceeding a few seconds per day were recorded. It is possible that the DOW time deviated from UTC by some *fixed* amount *different* than the believed 120 s, but this would not account for the variable time offset between the visually indicated and radar indicated times of tornado passage past particular locations. Since the outer edge of the debris cloud of the tornado sometimes exceeded 1 km in diameter (see later discussion), and the tornado was moving approximately 6 m s^{-1} (Table 1), it would require approximately 170 s for the tornado to traverse any particular location. Errors of ~170 s may

be inherent in the visual observations if there was ambiguity regarding whether reported times corresponded to the passage of the leading edge, center, or trailing edge of the visible debris cloud of the tornado. Visually indicated *center* crossing times might have been uncertain by at least 30 s (200 m or 0.2 visual debris cloud diameters), since determination of the precise center through the diffuse and changeable debris cloud might have been difficult (see Fig. 3, top).

The radar and visually determined tracks disagreed significantly during tornado dissipation. The DOW data

TABLE 1. Dimmitt tornado near-ground vital statistics.

Time (UTC)	Lat (°)	Long (°)	Range to center (m)	Azimuth to center (°)	Peak DOW-Indicated windspeeds (m s⁻¹)				Ground-relative motion of center (m s⁻¹)
					Raw Doppler	Adjusted for aspect ratio	Vortex rel.	Ground rel.	
0103:35	34.52038	−102.29010	2970	112	70	81	83	89	6.8
0105:12	34.52610	−102.28867	2920	99	74	88	89	95	6.6
0106:51	34.53193	−102.28706	3000	87	71	82	84	91	6.6
0108:28	34.53766	−102.28911	2930	74	65	78	77	82	4.8
0110:30	34.54264	−102.28807	3220	65	67	76	75	81	6.0
0112:09	34.54823	−102.28700	3580	57	65	78	75	81	6.1
0113:47	34.55352	−102.28658	3960	50	61	75	71	79	8.6
0115:27	34.56128	−102.28764	4510	41			—	—	—
0117:26	34.56290	−102.28834	4610	39			—	—	—

indicated that the tornado dissipated north-northwest of the Playa Lake (Fig. 2) while the visually determined track suggested northeast motion and dissipation to the northeast of the lake. This disparity was not surprising since the tornado was tilted and twisted at this time (see Fig. 3, bottom, and later discussion). During the dissipating stages of the tornado, there were times where no low-level condensation funnel was visually observable from the DOW site (Fig. 3, lower right). Visual observations might have focused on regions significantly above or below the lowest DOW radar scan levels. Precise visual observations were probably more difficult during this less visible dissipating stage of the tornado.

b. Motion

Before the DOW began observations, the tornado moved eastward, then northeastward. During the period of DOW observations the track was generally northward, with one significant deviation to the north-northwest from 0106:51 to 0108:28 UTC (Fig. 2). It is possible that this deviation to the north-northwest is similar to the wobbling motion often observed in hurricane eyes (Lawrence and Mayfield 1977; Willoughby and Chelmow 1982), and the shape of the tornado track suggests the possibility of trochoidal motion, but the relatively long repeat intervals between DOW low-level observations (100 s), preclude any definitive characterization. The ground-relative speed of the tornado center was variable within a limited range until near the time of dissipation, ranging from 4.8 ± 1.5 m s⁻¹ to 6.8 ± 1.5 m s⁻¹ (Table 1). Forward motion was constant within measurement error, between 6.0 ± 1.5 m s⁻¹ and 6.8 ± 1.5 m s⁻¹, except immediately following the north-westward shift between 0106:51 and 0108:28 UTC and during the tornado's final minutes, when the speed increased to 8.6 ± 1.5 m s⁻¹, then slowed significantly.

c. Reflectivity structure

The location of the DOW, so close to the tornado and within the hook echo of the parent thunderstorm, pre-

vented comprehensive observations of the tornado environment. The location of the tornado relative to the southern portions of the parent thunderstorm during the early and late portions of the observation period are illustrated in Fig. 6. The most striking features were the circular ring of debris at the tip of the hook echo, which extended to the right (south) of the scan, then behind the radar, and the strong velocity couplet associated with the tornado. The ring of debris was initially separated from the high reflectivity region of the parent supercell. However, the ring, together with the entire tornado, became more contiguous with the parent storm as the tornado weakened and dissipated. Severe attenuation complicated the interpretation of the large-scale reflectivity field. At 0103:45 UTC strong mesoscale convergence and rotation in the gust front appear to be present at 10-km range to the east of the DOW (near the top of the plot) at 350 m AGL. Peak values of azimuthal shear at 1000 m AGL (not shown) exceeded 0.01 s⁻¹ (50 m s⁻¹ over 3000 m). The region of apparent convergence and vorticity extended northwestward into an apparent updraft region to the area just north of the tornado. By 0112:19 UTC (Fig. 6, bottom), well before final dissipation of the tornado itself, this larger-scale feature weakened and appeared predominately convergent.

Expanded views of the reflectivity field of the tornado near the ground and at 1 km AGL are presented in Figs. 7 and 8 and expanded views of the Doppler velocity field are presented in Figs. 9 and 10. The nearly circular ring of debris, up to 800 m in diameter (distance from peak reflectivity to peak reflectivity) at low levels, and 200–300 m in thickness, surrounded the tornado at low levels during the entire observational period (Fig. 7). The outer edge was roughly coincident with the radius of >30 m s⁻¹ near surface winds (see Fig. 9). However, changes in the diameter of the ring through most of the observation period were not well correlated with changes in velocity structure. For example, the ring shrunk to approximately 400-m diameter at 0107:01 UTC (Fig. 7c) then expanded to 800 m, but there was no corresponding contraction/expansion or weakening/strengthening in the velocity pattern (Fig. 9c). At times (e.g., 0107:58 UTC; Fig 8d) there were indications of con-
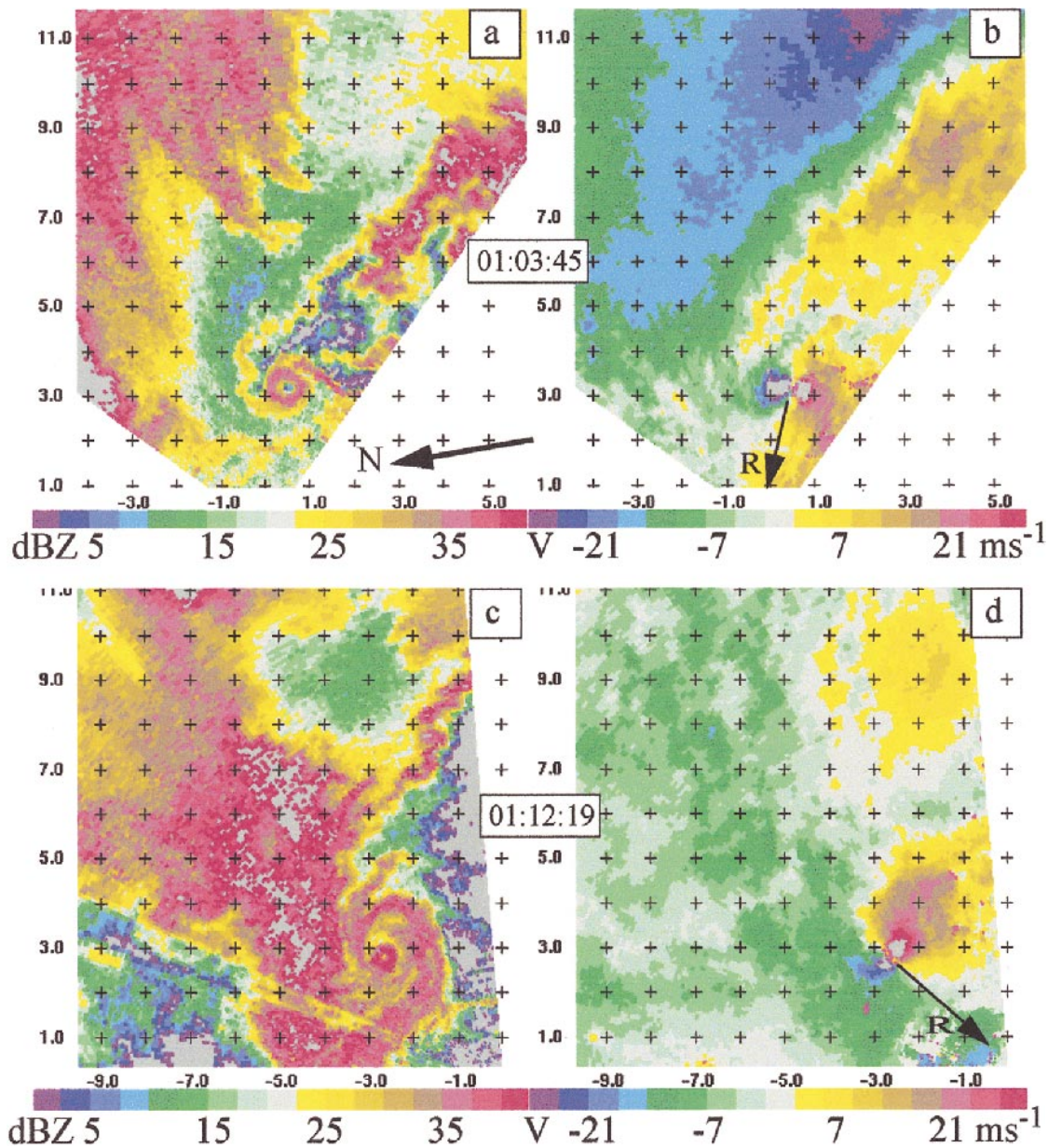
FIG. 6. View of tornado and southern portion of parent thunderstorm during (a), (b) mature (0103:45 UTC) and (c), (d) dissipating (0112:19 UTC) stages. Data from 2° elevation angle scans. At the earliest times the hook echo, well separated from the parent thunderstorm, is partially visible. At later times, rain, exhibiting high reflectivity has surrounded the tornado. Low reflectivity behind the tornado is an artifact of attenuation. Doppler velocities reveal the intense tornado couplet and the strong mesoscale circulation to the east at early times and only the tornado couplet at later times. Reflectivity is in dBZ and velocity is in m s^{-1} and tick marks define a grid with 1-km spacing. Arrows marked ''R'' indicate direction of DOW.

centric rings/spiral bands that might have been caused by the tornado encountering productive sources of debris at particular instants. The debris might then have been centrifuged outward and upward in conical patterns, resulting in the observed rings/bands. High reflectivity rings/bands outside the debris ring were probably caused by raindrops spiraling around the tornado. As the tornado weakened and occluded, these features became dominant and the debris ring contracted. By

0114–0115 UTC the debris cloud was difficult to discern (Fig. 8h) except at the surface (Fig. 7h) where it had a diameter of only 500 m. This was associated with a gradual weakening of surface winds (Fig. 9) and shrinking of the radius of winds >30 m s^{-1}.

While low reflectivity regions have been associated with tornado observations for decades (Fujita 1958; Wakimoto and Martner 1992; Wakimoto et al. 1996), this is the first time that a small-scale eye, explicitly
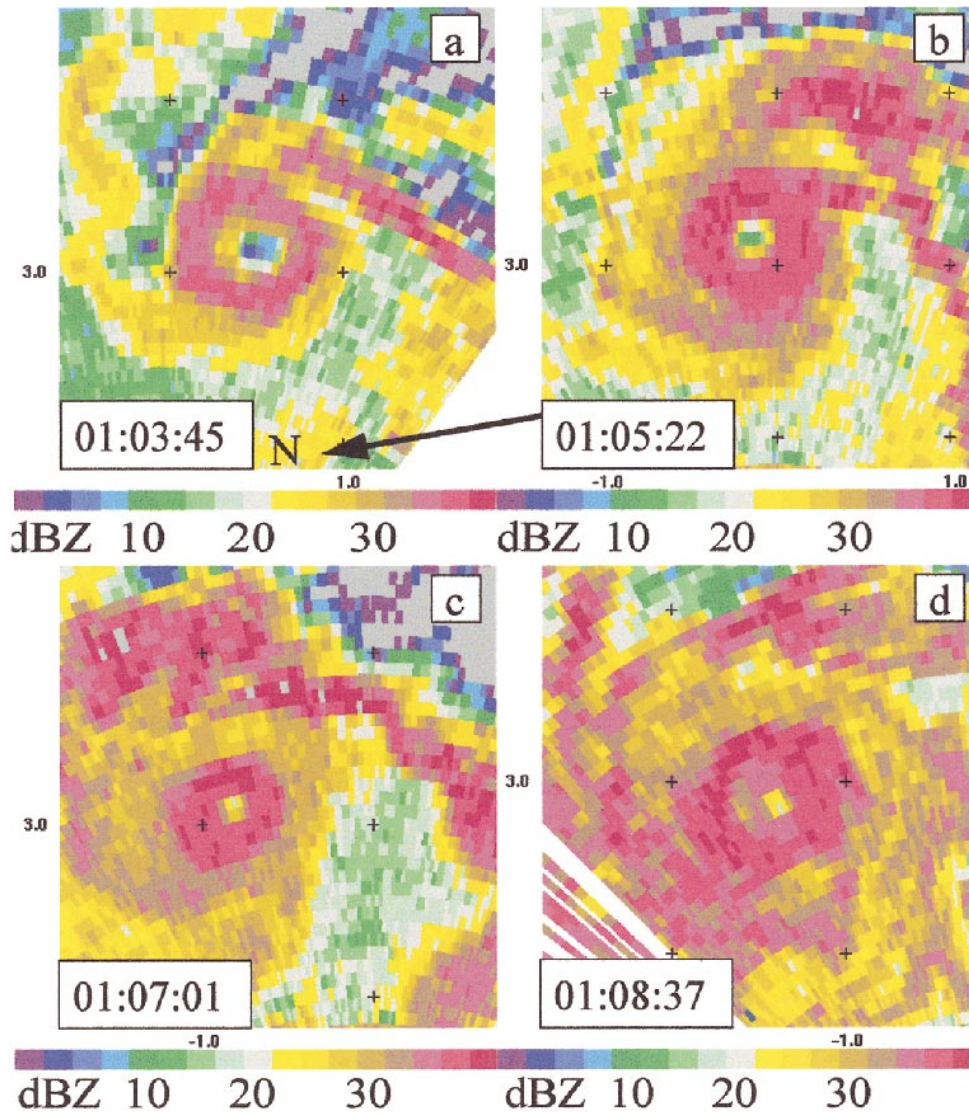
FIG. 7. Radar reflectivity of tornado at low levels from 2° elevation scan. Altitudes of radar beams at center of tornado were approximately 100 m at the earliest times, increasing to 150 m at the latest observation time. The distinct nearly circular ring, diameter = 800 m, of debris was clearly separate from surrounding rain

bounded by a debris cloud caused by the tornado circulation, separate from the coiled portion of the hook echo, has been resolved. It is likely that the low reflectivity regions observed in previous, lower-resolution, studies were manifestations of a reflectivity minimum at the coiled tip of the hook echo bounded by semiconcentric rings/spiral bands of precipitation particles, not the smaller debris cloud associated with the tornado. The observed low-reflectivity regions were likely analogous to the region bounded by the rings/bands observed outside the debris cloud of the Dimmitt, Texas, tornado (see Figs. 5c, 7d, 7e, 7f, and 8d). With low resolution data, the small ring of debris and very small eye visible in Figs. 6c, 7b, 7c, 7e, 7f, and 7h would be unresolved. Low resolution data from the time of Fig. 7c would have resolved only the larger low reflectivity

region to the east (above in the figure) of the debris cloud, about 300 m away from the tornado center. In Wakimoto et al. (1996), the high reflectivity surrounding ring is 3 km in diameter, much larger than the probable debris/centrifuged precipitation particle column of the tornado. In Fujita (1958), data resolution precludes determination of the nature of the ring or eye. Wakimoto and Martner (1992) present a high reflectivity ring with a diameter of 800 m, similar in scale to what was observed in the Dimmitt tornado. However, the low reflectivity region inside is characterized, probably, by only one or a few radar measurements (300 m × 300 m × 150 m scale) and it appears, visually, that the tornado is of a much smaller scale than the Dimmitt tornado. It is therefore unclear whether the high reflectivity is associated with the coiled tip of the hook echo
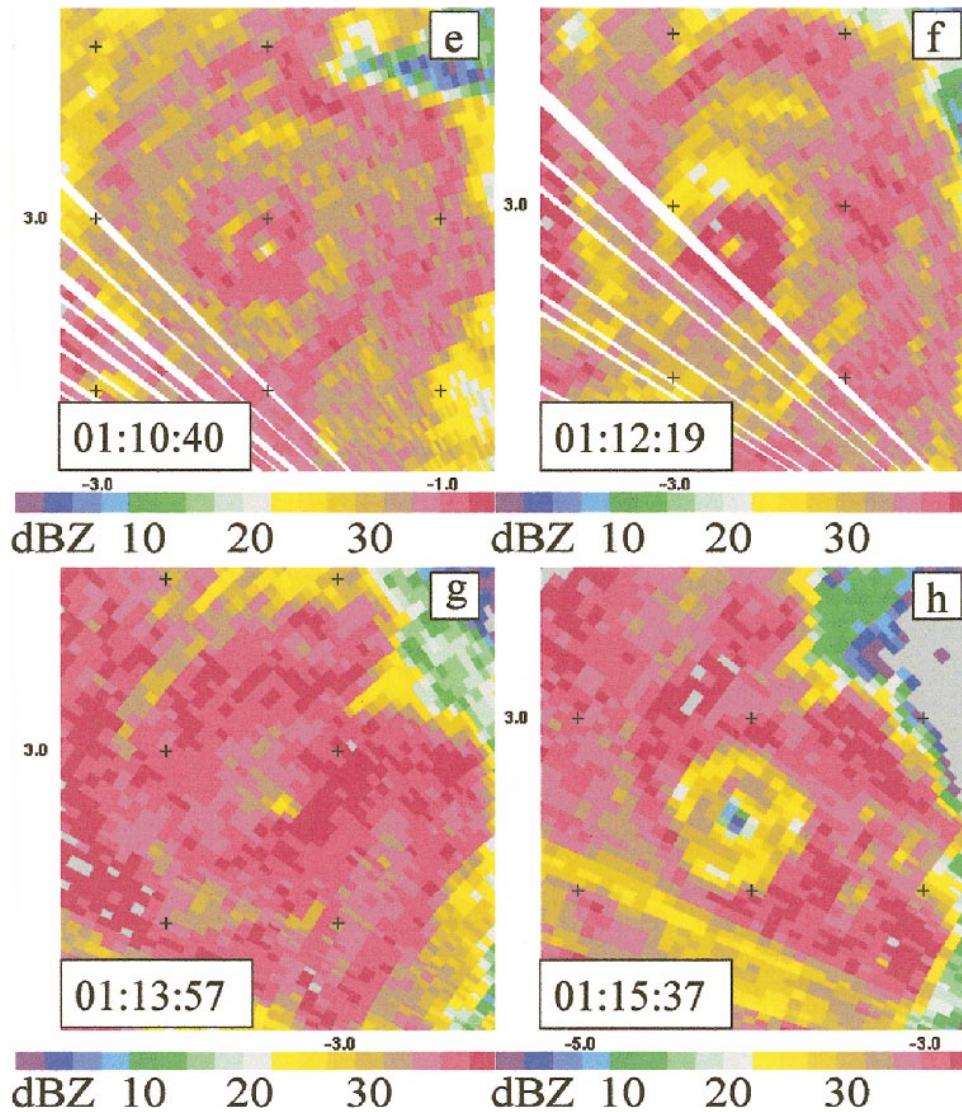
FIG. 7. (*Continued*) echoes at the earliest time (a), but gradually became surrounded by rain. (g), (h) The debris cloud was less discernible and smaller as the tornado dissipated in the later observations. Reflectivity is uncalibrated dBZ and tick marks define a 1-km grid.

or the debris cloud and/or centrifuged precipitation field of the tornado itself.

At the highest levels observed by the DOW, near 1 km AGL, the tornado was still evident as a ring or several concentric rings of high reflectivity with diameters of 1.0–1.8 km (Fig. 8). At later times, after 0107 UTC, vertical cross sections (discussed later) suggested that this reflectivity was probably caused by raindrops rather than debris. The debris rings visible at 0103:13 and 0104:41 UTC (Figs. 8a,b) exhibited 15–30 dB less reflectivity than at the ground (Figs. 7a,b). Arcs of high reflectivity were occasionally visible inside the raindrop rings, for example to the east of the tornado center at 0107:58 UTC (Fig. 8d). It is likely that these were caused by puffs of high reflectivity debris lofted from the ground. A curtain of rain extended from the

central rings eastward, then southeastward along the axis of the major inflow into the storm (see also Fig. 6) until at least 0111:36 UTC (Fig 8f), after which the reflectivity associated with the tornado was more contiguous with the main reflectivity body of the parent storm. As the tornado dissipated, at upper levels first (see following discussion), the eye became wrapped completely by high reflectivity rain and the entire structure contracted and was surrounded by the high reflectivity portion of the parent thunderstorm.

d. Velocity structure

Low- (below 100 m AGL) and high- (near 1 km AGL) level Doppler velocity data in the tornado revealed an intense velocity couplet (Figs. 9 and 10) with
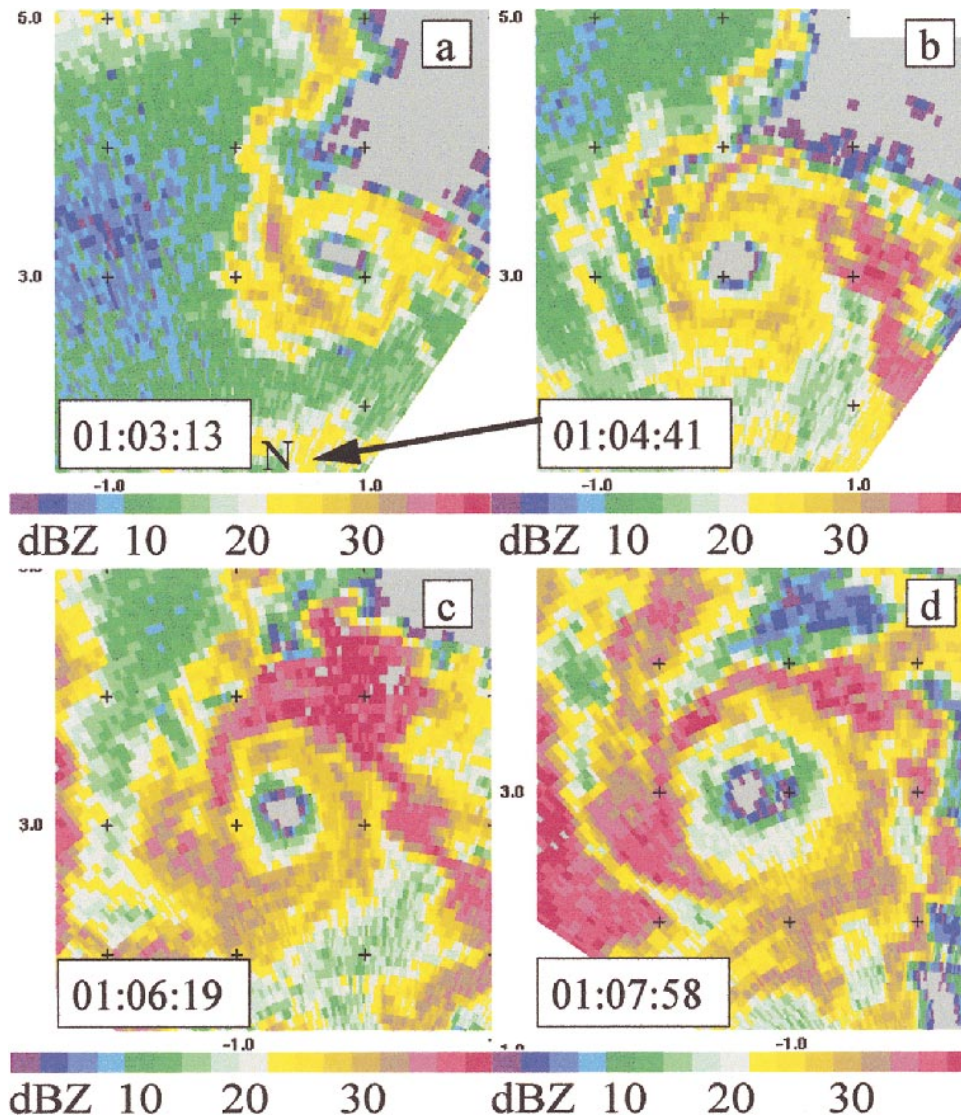
FIG. 8. As in Fig. 7 but data from DOW scans closest to 1 km AGL at the center of the tornado. (a) Reflectivity due to rain and debris can be seen surrounding the tornado at the earliest observation time. (g), (h) Rain enveloped the tornado, which became incorporated into a general field of high reflectivity in the

extremely high azimuthal shear (Fig. 11). The basic structure near the ground and at 1 km AGL remained dominated by the main vortex throughout the period. The strength of the circulation weakened markedly at 1 km AGL in the later scans (Figs. 10e–h). Strong winds extended well beyond the main vortex with wind speeds >40 m s^{-1} over 1 km to the east of the center at 0105:22–0107:01 UTC (Figs. 9b,c), and >30 m s^{-1} over a broad region 500–1500 m from the tornado center at several other times. The slow decay of the wind speed away from the center of the tornado will be discussed in section 3f.

The rate of decay of the winds away from the tornado was not monotonic. As evident in Figs. 9b,c and suggested in some other scans (Figs. 9g and 10g), there were secondary maxima or regions where the wind speed did not decay with increasing distance from the center of circulation at ranges of 500–1000 m from the center of the vortex. (These were also evident in analyses of observations near 1 km AGL; see discussion of central downdraft later.) In the intense main circulation of this tornado, prominent secondary maxima were often not present, but strong secondary maxima with similar structure had been observed in two other tornadoes. It is possible that these secondary maxima were evidence of spiraling inflow with parcels containing characteristic but differing initial angular momentums causing an onion-skin-like structure as they converged toward the tornado center. In order to evaluate this hypothesis, dual-Doppler vector wind observations, from which the an-
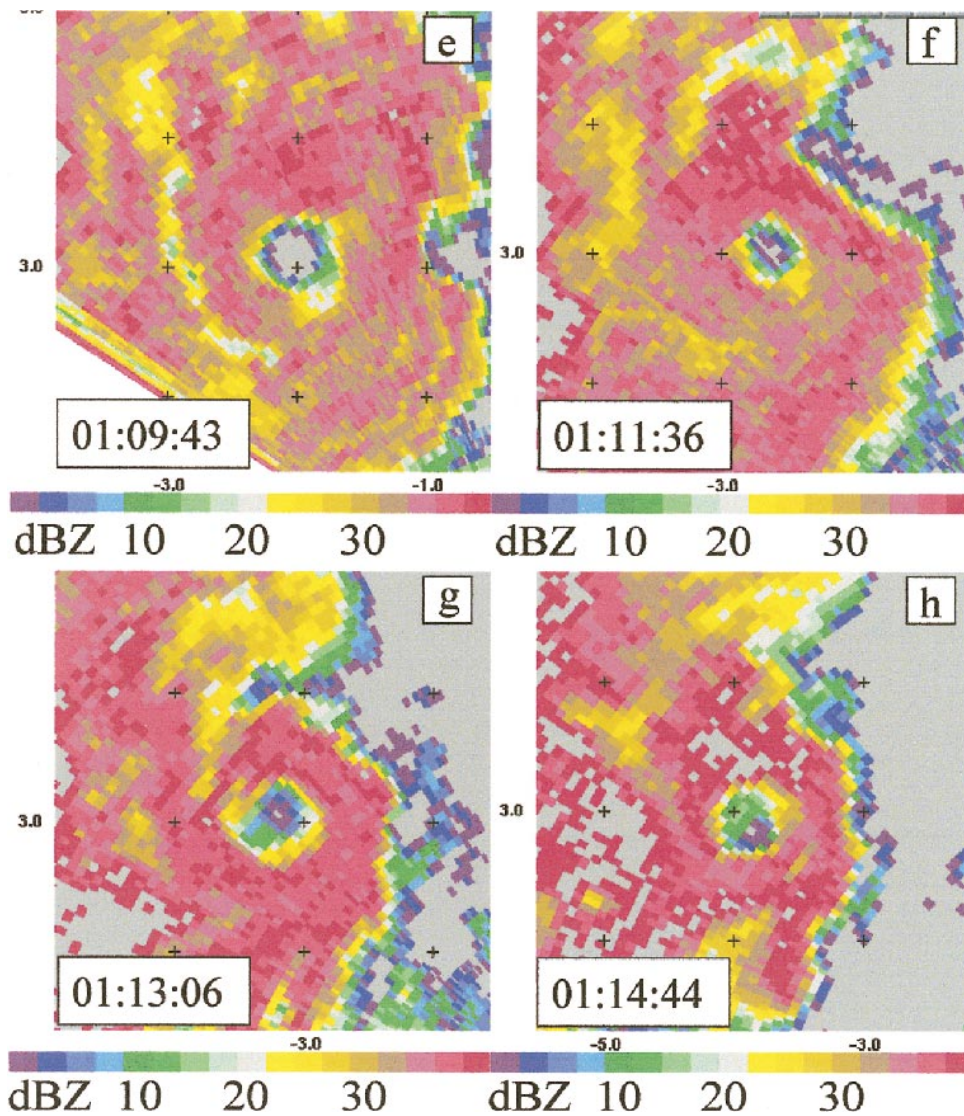
FIG. 8. (*Continued*) parent thunderstorm by the latest times. (d) At times, an inner ring or partial ring of debris was visible inside the outer rain rings. Less debris was visible in the later observations (e)–(h) since it was confined mostly to lower levels.

gular momentum of individual parcels can be deduced, may be required.

Suction vortices of the type documented by Fujita (1970), Ward (1972), and Davies-Jones (1986) were not observed in the velocity data. The velocity couplets were striking in their simplicity and lack of small-scale variation around the tornado. They appear remarkably like those calculated by Wood and Brown (1997). It is likely that such features were of an unobservable scale in the case of the Dimmitt tornado. One of the authors (JW) observed small-scale damage patterns in agricultural fields. These had apparent radii of curvature of approximately 10 m, but were not systematically documented. Cycloidal marks with a larger, approximately 75 m, scale were observed in aerial photographs by Rasmussen and Crosbie (1995). Resolution of the caus-

ative wind field features by the DOW prototype at a range of 3–5 km would have been difficult or impossible.

Peak observed azimuthal shear values were typically near 0.6 s^{-1} in the earliest scans dropping to 0.4 s^{-1} later (Fig. 11), implying relative vertical vorticities above 1.0 s^{-1}. Shear values in the lowest 300 m of the tornado, observed with the $1°$, $2°$, $4°$, and $6°$ elevation angle scans, were typically larger, near 0.6–0.7 s^{-1}, implying relative vertical vorticities near 1.3 s^{-1}. These are believed to be the largest observed in a vortex of this size [cf. 0.46 s^{-1} from Wakimoto et al. (1996)]. (With aspect ratio corrections, discussed later, the data suggested that the actual peak values of shear and vertical vorticity at low levels were about 20% higher, near 0.9 and 1.8 s^{-1}.) Since peak azimuthal shear values
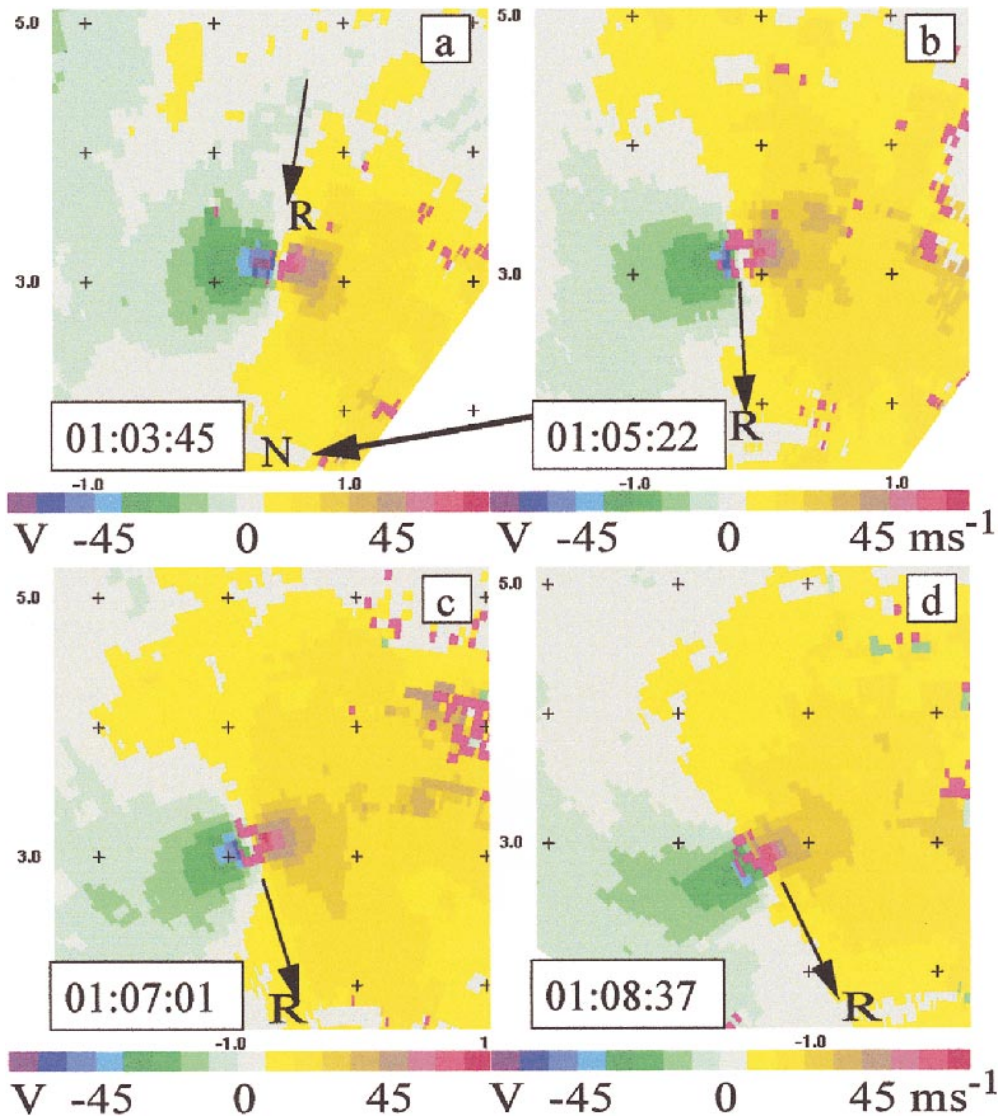
FIG. 9. Doppler velocity in tornado at low levels from 2° elevation scan. Radar beam altitude at the center of the tornado was approximately 100 m AGL at the earliest times, increasing to 150 m AGL at the latest observation time. Intense velocity couplet of the tornado was evident at all times. Peak Doppler velocities were in excess of 70 m s^{-1} at the earliest times, decreasing to 60 m s^{-1} at the latest times, with peak azimuthal shears

depended strongly on the dealiasing of individual data points near the center of the tornado, occasional peak values of nearly 1.0 s^{-1}, implying vertical components of vorticity over 2.0 s^{-1}, should be regarded with skepticism. There was no clear dependence of peak azimuthal shear with height.

Doppler velocity differences, ΔV, across the tornado exceeded 139 m s^{-1} at the earliest observation times at approximately 60 m AGL. A time–height cross section of ΔV values interpolated to a Cartesian grid is presented in Fig. 12. (Values were interpolated to a Cartesian grid using the NCAR REORDER software. Radar data were interpolated to a 50-m grid using nearest neighbor interpolation. The vertical spacing between most scans was approximately 100–130 m at the range of the tor-

nado, so there were few gaps. When gaps were present, linear interpolation was used for the purposes of calculations of areas and volumes containing winds over the 40 m s^{-1} threshold.) Values of ΔV generally decreased with height, above a surface friction layer, at all observation times, as predicted by conceptual and computer models (Lewellen 1993). Peak ΔV values were always found below 250 m AGL. With time, ΔV decreased both at low levels and at higher levels, but, as suggested by Brandes (1984), the decrease was most pronounced at higher levels. Values of ΔV dropped by only about 25 m s^{-1} at 50–100 m AGL during the observation period, but decreased by about 40 m s^{-1} at 800 m AGL. Thus, ΔV values less than 80 m s^{-1} were common at approximately 1 km AGL after 0109 UTC
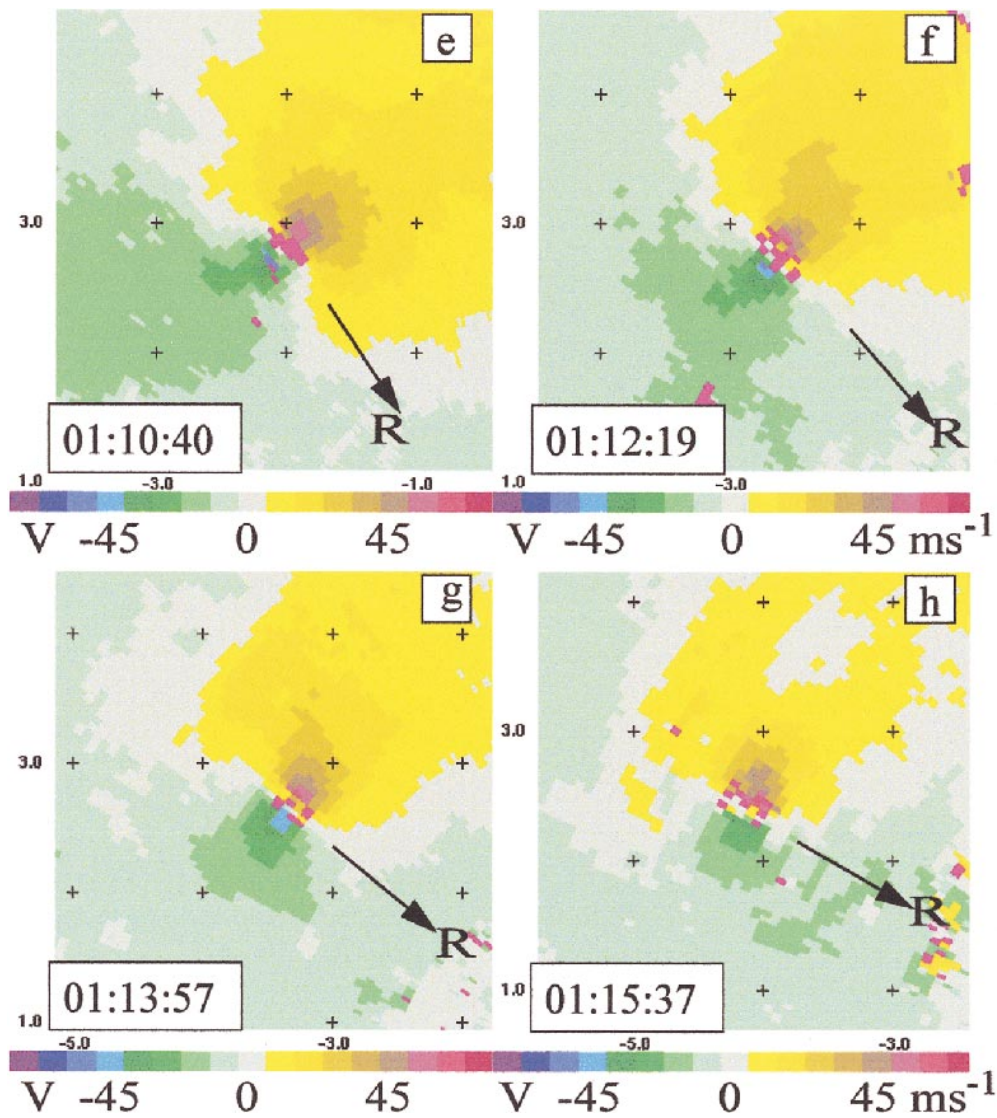
FIG. 9. (*Continued*) near 0.6 s^{-1} at the earliest times decreasing to 0.4 s^{-1} at the latest times. No unambiguous subtornado-scale features or suction vortices were evident at any time. Velocity scale is in m s^{-1} and tick marks define a 1-km grid. Arrows labeled "R" indicate direction to the DOW. Bright pink/lavender values are those that have been filtered out due to noise or clutter.

while strong values >105 m s^{-1} persisted at 50–200 m AGL.

These data revealed that a small-scale, intense, as measured by ΔV, tornado circulation persisted but the tornado as a whole contracted significantly. Peak ΔV (at the shrinking tornado core) remained constant while the tornado circulation apparently lost total angular momentum. This implied loss of momentum occurred not just at the tornado core, but extended to a radius of several hundred meters from the circulation center as the entire circulation away from the core radius weakened. While peak velocity (usually inferred from damage surveys) is most commonly used to characterize tornado strength, another indicator of total tornado strength, the area within which $|V| > 40$ m s^{-1} (Fig. 13),

revealed a more drastic decrease in tornado strength at all levels, particularly above 500 m AGL. At the earliest observation time, the area with winds >40 m s^{-1} was almost 180 000 m^2 at 50–100 m AGL, decreasing to 100 000 m^2 at 1000 m AGL. While ΔV calculations suggested that the peak winds at 50–100 m AGL had only dropped by about 15% by 0113 UTC, the area near the surface impacted by vortex relative winds >40 m s^{-1} had decreased by about 70% to about 50 000 m^2. The dissipation at 1000 m AGL was even more striking with winds in excess of 40 m s^{-1} affecting areas of less than 10 000 m^2, a decrease of over 90%. Volume integrated calculations (Fig. 14) illustrated that the height averaged peak winds in the tornado dropped by 20%, from 118 to 93 m s^{-1}, while the volume affected by
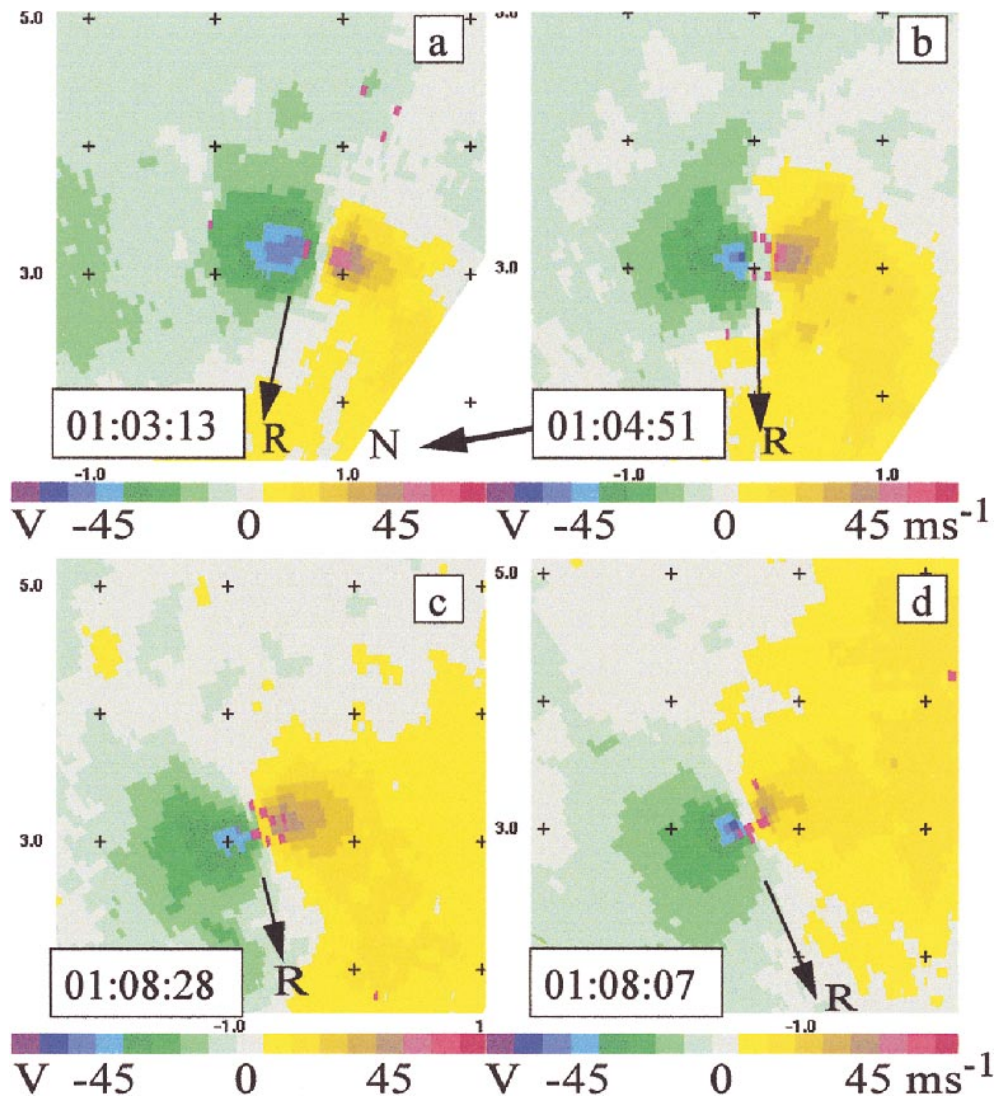
FIG. 10. As in Fig. 9 but for DOW scans closest to 1 km AGL at the tornado center. The intense cyclonic Doppler velocity couplet was visible at the earliest times, but decreased in intensity as the tornado dissipated aloft. Peak Doppler velocities were near 70 m s^{-1} at the earliest times, but decreased to near 40 m s^{-1} later. There was some evidence of multiple wind maxima away from the primary maxima at (b), (d) early times and

winds >40 m s^{-1} dropped by about 70% from 1.2×10^8 m^3 to less than 4×10^7 m^3. (It is interesting to note that this high wind region was smaller than a single radar resolution volume of the KLBB radar: 10^9 m^3.) This, combined with the fact that peak winds at the tornado core were relatively constant, implied that there was a drastic drop in total angular momentum while peak surface wind speeds remained comparatively constant. Due to the resultant small scale of the weakening tornado, radar beam blockage, and the short timescale associated with final dissipation, the final decay of the tornado, which might have occurred during the 100-s interval between low-level radar scans, was not observed by the DOW. (The choice of 40 m s^{-1} as a discriminator was relatively arbitrary, but roughly corre-

sponded to the visual size of the tornado and the debris cloud at the surface and an approximate threshold for damage-capable winds. The conclusions would be similar if other values, for example, 35 or 50 m s^{-1} were presented.)

One of the most striking structures to be observed in this tornado was a central downdraft. This downdraft was observed only in the earliest scans. It is important to note that this was a *direct observation of particle Doppler velocities, not a calculation based on the integration of mass continuity* such as that found in Wakimoto and Martner (1992) and elsewhere. Doppler velocity observations in the downdraft region are presented in Fig. 15. In the highest elevation scans, 10°, 12°, 14°, and 18°, there was a roughly 150-m diameter
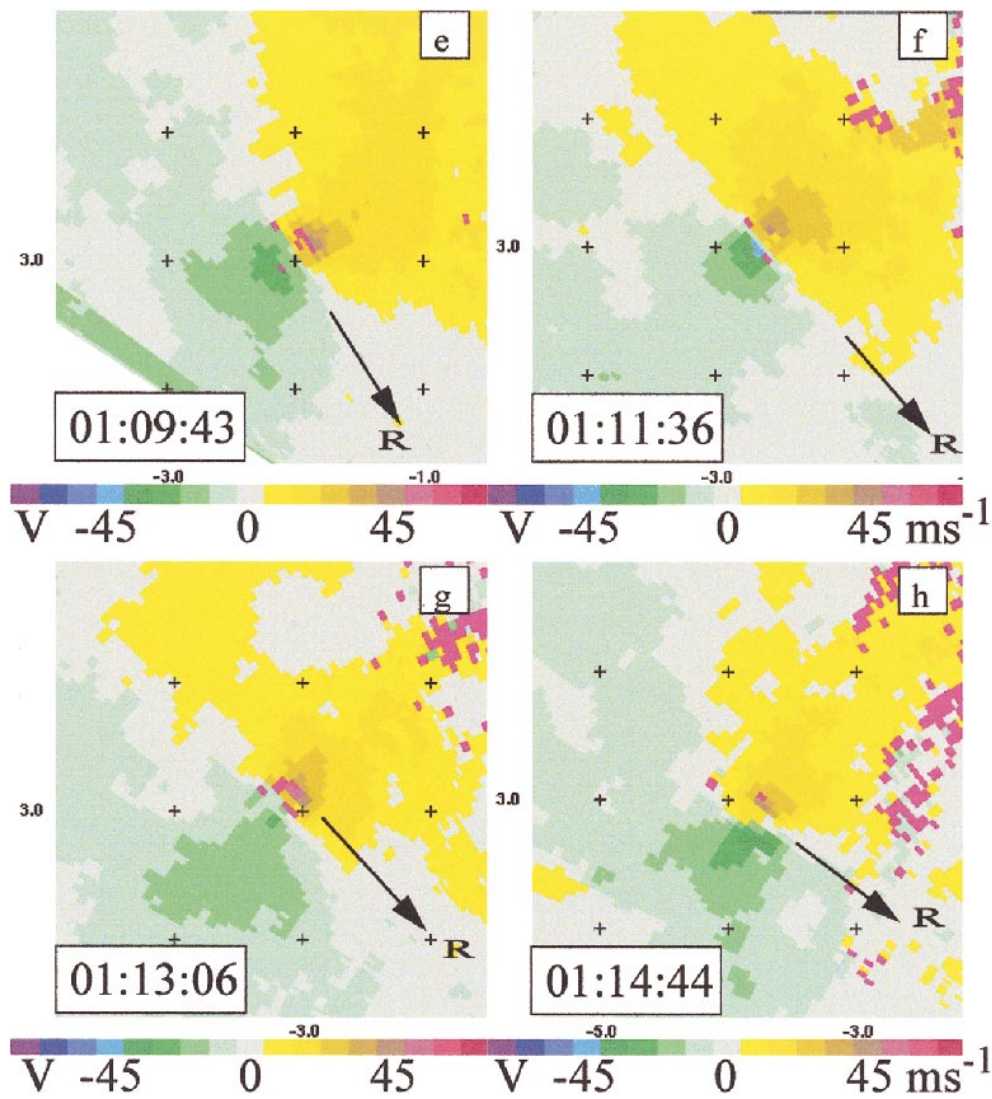
FIG. 10. (*Continued*) (g) at later times. Velocity scales are in m s^{-1} and the tick marks define a 1-km grid. Arrows labeled ''R'' indicate the direction to the DOW. Bright pink/lavender values are those that have been filtered out due to noise or clutter.

region with relatively constant Doppler velocities of -7 to -10 m s^{-1} (toward the radar). The region was smaller in the 8° scan (400 m AGL) and not present in the 6° scan (300 m AGL) or lower. (Note also the secondary wind maxima, 1000 m away from the tornado center, that are particularly evident in the 14° scan.) The tornado was moving nearly tangentially to the DOW at this time (see Fig. 2), so tornado motion toward or away from the radar was not the source of these velocities. The vertical component of the scatterer motion, W_p, could thus be directly calculated from $W_P = V_{\text{Doppler}}/\sin(e) = 30 \pm 10$ m s^{-1}, where e is the elevation angle of the radar beams above the horizon. Since reflectivity values in this region were very low, and centripetal accelerations large [roughly, $V^2R^{-1} = (70 \text{ m s}^{-1})^2 (100 \text{ m})^{-1} = 50$ m s^{-2}, where R is the radius from the center of the tornado], it is likely that the region was almost devoid of large scatterers with appreciable terminal velocities, so W_P approximated the actual air parcel downdraft velocity. It is believed that this was the first time such a structure has been directly observed in an actual tornado. NCP values were typically 0.3–0.5 in the downdraft region, probably due to the weak reflectivity. The smoothness of the Doppler velocity field suggested that the flow was not extremely turbulent. The downdraft disappeared after 0105 UTC. The tornado was probably a partial-two-cell vortex (Fig. 16c) with a downdraft penetrating to 400 m AGL, as described in Davies-Jones (1986) from 0104 to 0105 UTC and a single-cell vortex (Fig. 16b) thereafter until dissipation. The DOW observations could not exclude extremely narrow (<50–100 m) or short-lived (<100 s) downdrafts, at other
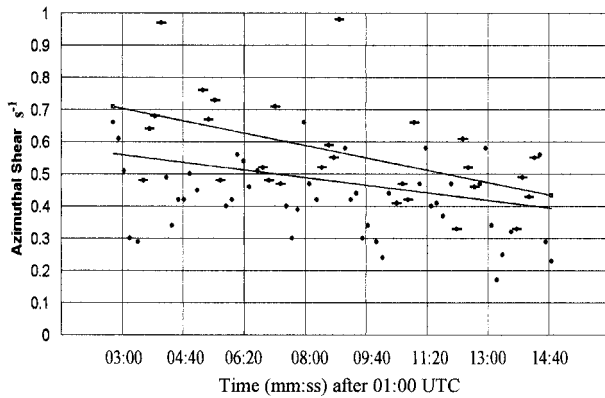
FIG. 11. Measured azimuthal shear versus time. Shear values for every scan are plotted. There was a general trend toward weaker shear as the tornado dissipated while contracting, but there was still very strong shear up until near dissipation. Shear values from lowest elevation angle scans, $1°$, $2°$, $4°$, and $6°$ (with lines through points), were typically higher, near $0.6–0.7$ s^{-1}, at the earliest observation times. Top line represents best fit linear trend of lowest elevation angles, bottom line from all observations. Values not adjusted for aspect ratio.

times. A downdraft structure of similar horizontal size was reported in simulated tornadoes by Lewellen et al. (1997); however, peak downward velocities were found closer to the ground in the simulations. It it important to note when making these comparisons that the diameter of the observed low reflectivity eye (Fig. 7), probably caused by both downdraft and centripetal effects, was larger than the diameter of the observed downdraft region (Fig. 15). It is also important to note that our observations only extend to approximately 1 km AGL. It is quite possible that the downdraft structure terminated above 1 km AGL, and the tornado actually had a more complex structure (Church and Snow 1993; Church et al. 1979; Fiedler and Rotunno 1986).

There are alternate possible explanations of these observations, which, while not strictly falsifiable with the current observations, appear unlikely. It is possible that a very few large scatterers, with large terminal fall speeds (~30 m s^{-1}) could have caused the low reflectivity in the eye, and contaminated the observations. This possibility is discounted since the Doppler velocity and reflectivity fields were smoothly varying, with the amplitude of the downdraft increasing with increasing altitude. The values are relatively constant across the eye. Furthermore, such large particles would have been most susceptible to centrifugal removal from the eye. Additionally, the spectral width values were low, which probably would not have been the case if a few large objects of debris caused the observed reflectivity. It is also possible to postulate that a pathological contamination by sidelobe coupling from the high reflectivity region surrounding the eye caused the negative Doppler velocities. But, the smooth decrease of Doppler velocity with height and smooth horizontal variation made this less likely than the existence of a downdraft. Finally,
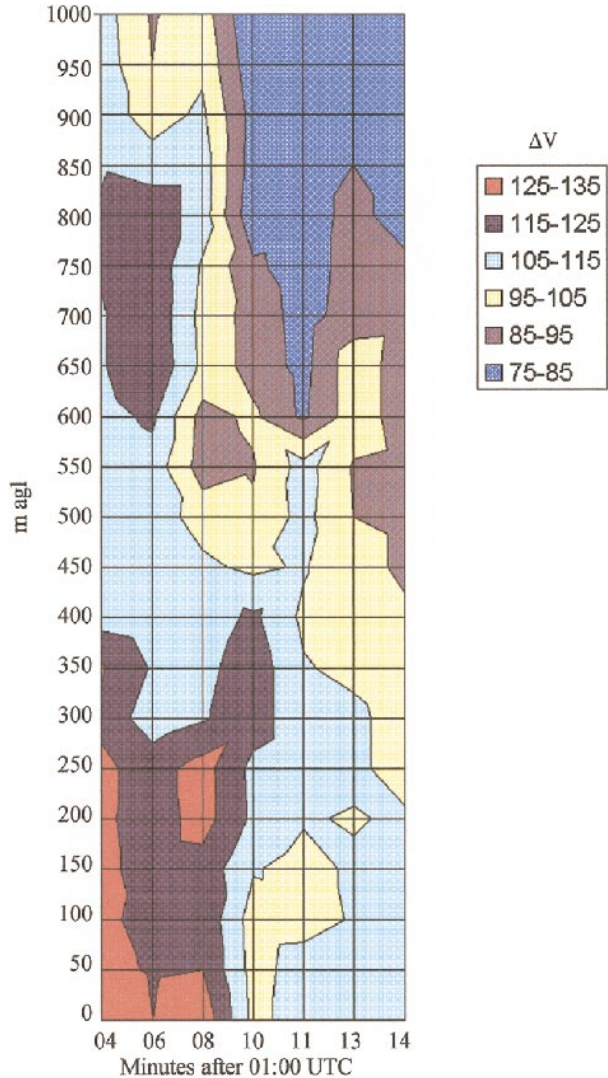

FIG. 12. Difference in Doppler velocity across tornado as function of time and altitude. Strongest differences were found at the earliest times at low levels. At the earliest times, strong differences were found up to 1 km AGL. At later times, surface values had decreased slightly, but values at 1 km had dropped by about 40%. Values not adjusted for aspect ratio.

the reflectivity inside the eye varied smoothly both vertically and horizontally. This would have been an unlikely result from the summation of power from various sidelobes, particularly as they impinged on significant debris in the surrounding ring. Contamination by horizontal motion of the tornado is ruled out since the radar-relative motion of the tornado was <1 m s^{-1}. It is possible to postulate a cross-vortex horizontal flow that could result in a negative Doppler velocity in the eye. But, the gradual decrease of Doppler velocity with height, and the abrupt cutoff below the breakdown level, are more consistent with a downdraft. No strong convergence or divergence was observed at the edge of the
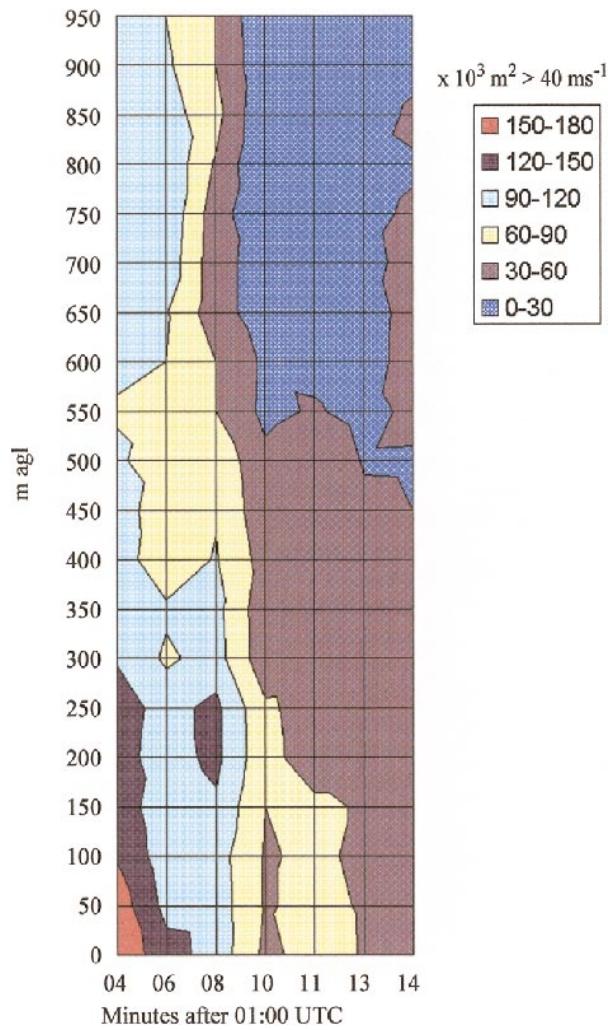
FIG. 13. Area impacted by high winds in excess of 40 m s⁻¹. Largest extent of high winds was at surface at earliest times when >40 m s⁻¹ extended over >150 000 m². At the surface this region decreased slowly to 75 000 m² by 0111 UTC, but at 1 km AGL, the area experiencing high winds dropped to almost zero by 0110 UTC. Even at the surface, the decrease of areal coverage was more significant than the decrease in wind difference across the tornado (Fig. 12). Values not adjusted for aspect ratio.
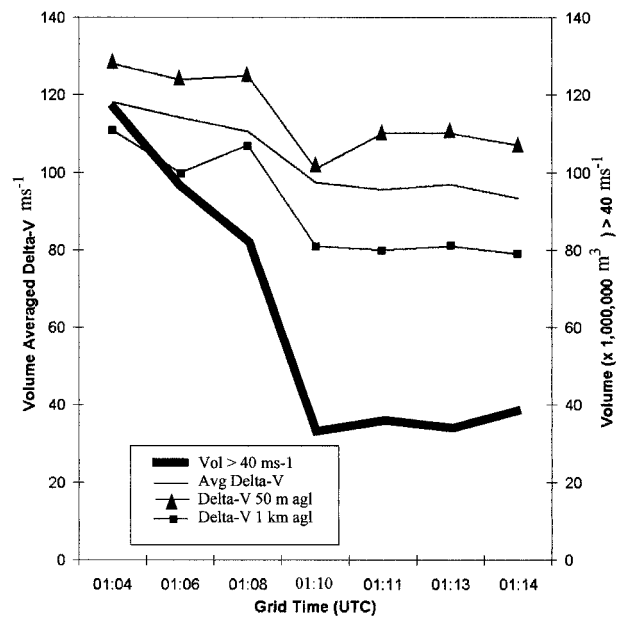

FIG. 14. Volume-integrated and -averaged tornado strength indicators as a function of time. While velocity differences decreased slowly near the surface and faster aloft, the decrease in the volume of atmosphere containing winds in excess of 40 m s⁻¹ was very rapid between 0104 and 0110 UTC. Values not adjusted for aspect ratio.

eye as would be expected if there had been strong cross-eye horizontal flow.

The vortex motion near the ground and at 1 km AGL were significantly different (Fig. 17), resulting in a time-varying inclination of the tornado. While the lowest levels of the tornado moved northward, northwestward, then northward again, the motion at 1 km AGL was more constantly northward until just before dissipation. Thus, the inclination of the tornado was generally to the west until 0109 UTC, then to the NE until dissipation. The tilting near dissipation was pronounced, nearly 45° or over 1 km horizontally between the ground and 1 km AGL (see also Fig. 3, lower left, though the inclination was largely away from the viewer and thus not

easily visible in the photographs). This may be an explanation of the disparity between VORTEX visual observations [probably of the 300–500 m AGL region of the tornado since the lowest portions may have been invisible (Fig. 3, lower right)] and the DOW-indicated near-surface track (near 100 m AGL).

Vertical cross sections through the radar data illustrate the vertical structure of the tornado. Cross sections were made by interpolating edited data onto a Cartesian grid with 50-m spacing using the NCAR program Reorder, then displaying the fields using NCAR's Zebra. Nearest neighbor weighting was used and tornado motion was determined subjectively from the velocity and reflectivity centers of the tornadoes in subsequent 1° elevation radar scans. With only bulk tornado motion removed, the resultant cross sections revealed the inclination of the tornado (Fig. 18, left). At the earliest observation times, the tornado was sloped upward toward the WNW (290°) with an angle of ~20° from the vertical in the lowest 450 m AGL, and about 10° from the vertical from 450 to 900 m AGL. This inclination was not perpendicular to the radar observations, but the Doppler velocity couplet was (see Figs. 9 and 10) since the flow was primarily vortical with little convergence or divergence (see section 3h). Therefore, artificial tornado motion was introduced into the interpolation scheme to force the resultant analyzed tornado to be nearly vertical (Fig. 18, right).

Cross sections through the reflectivity and velocity fields of the tornado at 0104, 0106, 0108, and 0110 UTC are presented in Fig. 19. At 0104 UTC, a high reflec-
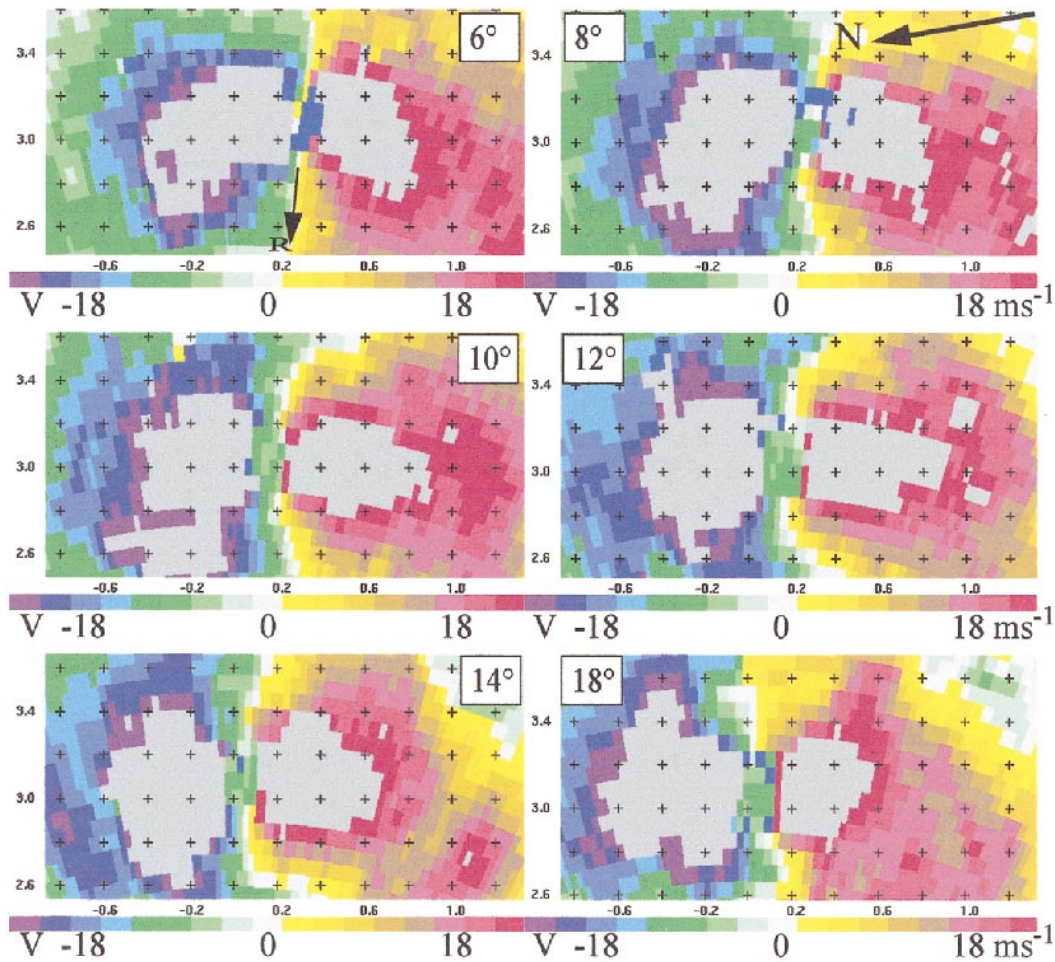
FIG. 15. Evidence of a downdraft at the center of the tornado. Doppler velocity in the center of the tornado in the highest scans at times 0104:04–0105:00 UTC. Velocity scale expanded to illustrate relatively constant downward motion in the downdraft. The downdraft was visible in all scans from (b)–(f) 8.0° to 18.0° elevation or from 400 m to 930 m AGL, but not present at (a) 6.0° or below. Dark blue values to the right of the downdraft were filtered due to low NCP, probably due to high shear or turbulence near the core flow radius of the tornado. (e) Note also the prominent secondary wind field maxima at 14°, 1000 m to the southeast and north of the center of the tornado. *Tick marks in this figure define a 200-m grid.* The velocity scale is in m s^{-1}. The arrow labeled ''R'' in the top-left panel indicates the direction to the DOW.

tivity debris cloud extended from the ground to over 700 m surrounding the low reflectivity eye. The outer edge of the debris cloud was roughly coincident with 30–35 m s^{-1} wind speeds. While initial lofting of debris was probably caused by turbulent flow associated with strong horizontal winds at the ground, continued lofting to great altitudes was likely caused by strong vertical motions within the debris cloud. The central downdraft is evident between 400 m and 1 km AGL as a region of 5–10 m s^{-1} negative (toward the radar) velocity. The lowest portion of the downdraft was coincident with a distinct narrowing of the reflectivity eye below 400 m AGL, further suggesting that the tornado structure approximated a partial two-cell vortex (Fig. 16c). There was a second narrowing of the eye at 100 m AGL, which was not correlated with any observed velocity structure. There were suggestions of wavelike patterns in the inner

edges of the debris cores. These were particularly visible on the left debris wall at 0104 UTC and in both debris walls at 0106 UTC. These appeared to be similar to the ''centrifugal waves'' presented by Church and Snow (1993), but might also be artifacts of antenna navigational errors. The horizontal amplitude was about 50 m, similar to the radar beamwidth. Further examination of future tornadoes is required to confirm the existence of and further characterize these structures. The altitude to which significant amounts of debris (>40 dBZ) were lofted decreased sharply from 700 m at 0104 UTC to less than 200 m at 0110 UTC. Since the tornado was passing over relatively homogeneous farmland to the southeast of Dimmitt during this period (Fig. 2, Fig. 3, top), the characteristics of available debris probably varied little over the several-minute time period. (However, it was possible that concentric reflectivity cones might
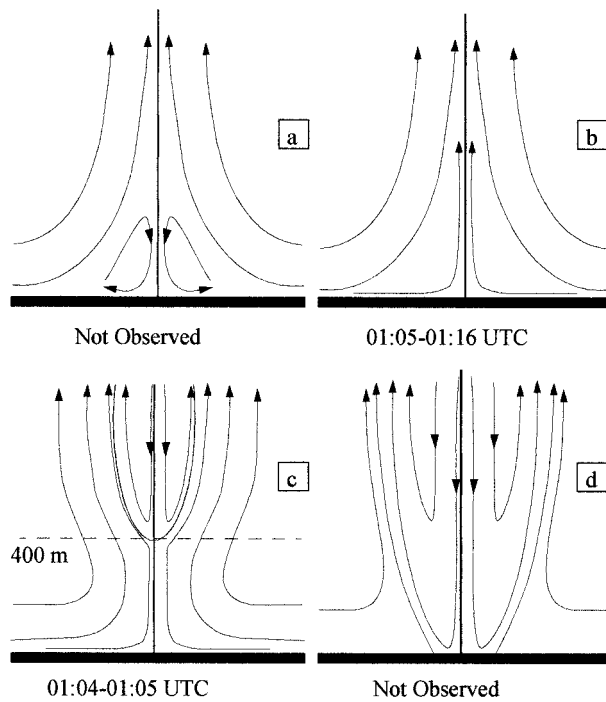
FIG. 16. Structure (adapted from Davies-Jones 1986) of the 0–1 km AGL layer of the Dimmitt tornado. At the earliest observation times, the tornado exhibited a partial two-cell structure similar to type c. At all other times, it appeared to be a single-cell vortex similar to type b.

have been caused by brief pulses of increased debris originating from either point sources at the ground or from suction vortex type structures.) Since peak surface winds decreased little during this period (Table 1; Fig. 14), it appeared that the area impacted by high winds (Fig. 13) and the altitude to which high winds extended (Figs. 12 and 13) were more important factors in determining how much debris was lofted to great altitudes, than merely the peak near-surface wind speed or F-scale rating. This could have important implications for debris transport studies (Levison 1997), particularly since peak winds, in the form of Fujita-scale ratings, are the most commonly used stratification criteria in tornado studies. Unfortunately, vertical wind speeds outside the eye could not be estimated. The Doppler velocity cross sections revealed the expected general decrease of wind speed with altitude (somewhat exaggerated by noncollocation of the cross sections and maximum observed Doppler velocities at all altitudes). At 0104 UTC, when the tornado was a partial two-cell vortex (Fig. 16c), the peak winds were separated by as much as 500 m aloft, but at later times, the peaks were closer together. The weakening of the tornado aloft was indicated by the absence of winds >40 m s^{-1} above 800 m at 0110 UTC. Secondary wind field maxima present aloft at 0104, 0106, and 0110 UTC were due to transient features in the wind field. They were not represented in the area-

and volume-integrated data presented in Figs. 13 and 14.

e. Asymmetry

Peak vortex-relative wind speeds on each side of the tornado vortex differed significantly, but wind differences on opposite sides of the vortex were much smaller than peak tangential speeds. Differences between the positive (away) wind speeds (on the rear-flank downdraft, or southern and southeastern, side of the tornado) and the negative (toward) wind speeds (on the updraft, or northern and northwestern, side of the tornado), relative to the vortex, showed a systematic bias toward positive values, particularly at later times at the highest observed levels (Fig. 20). The wind speed differences on opposite sides of the tornado sometimes exceeded 20 m s^{-1} and were typically 5–10 m s^{-1}. Wind speeds on the eastward side of the tornado (away) would have been slowed slightly more by frictional effects near the ground since they were associated with higher ground-relative speeds, driving the measured asymmetry more negative. *Thus, frictional effects do not explain the asymmetry.* Data from all periods showed a trend toward symmetry with increasing altitude at low levels, up to 800 m AGL. But, after 0110 UTC, and above 1 km AGL, wind speeds were much stronger on the southeastern (away) side of the vortex, but the circulation had weakened considerably and this statistic might have been dominated by flow not directly associated with the tornado.

f. Comparisons with idealized vortex

A commonly used conceptual model for a tornado (Zrnic and Doviak 1975; Burgess et al. 1993; Bluestein et al. 1993; Wood and Brown 1997) predicts that the velocity structure of the tornado should approximate that of a Rankine vortex where velocities inside a core radius R_0 are proportional to the distance to the center of the vortex and then decay inversely with distance outside this radius ($V \sim R$ for $R < R_0$ and $V \sim R^{-1}$ for $R > R_0$, where R is the distance from the center of the tornado). The currently presented DOW observations provided the first tests of this prediction in an actual tornado. It is likely that the sharp wind field maximum cusp predicted by the Rankine model at R_0 was unrealistic since turbulent diffusion of momentum would act to eliminate the cusp. Comparisons of high-resolution measurements to more realistic models, such as the Burgers–Rott vortex (Burgers 1948; Rott 1959), would be useful. Unfortunately, without vector wind field observations to determine convergence or radial inflow, it was problematic to calculate the idealized wind flow.

The Doppler velocity structure across the tornado was retrieved for 75 constant elevation sweeps. Various theoretical profiles were matched to the observed profiles outside of the core radius. The flow inside the core
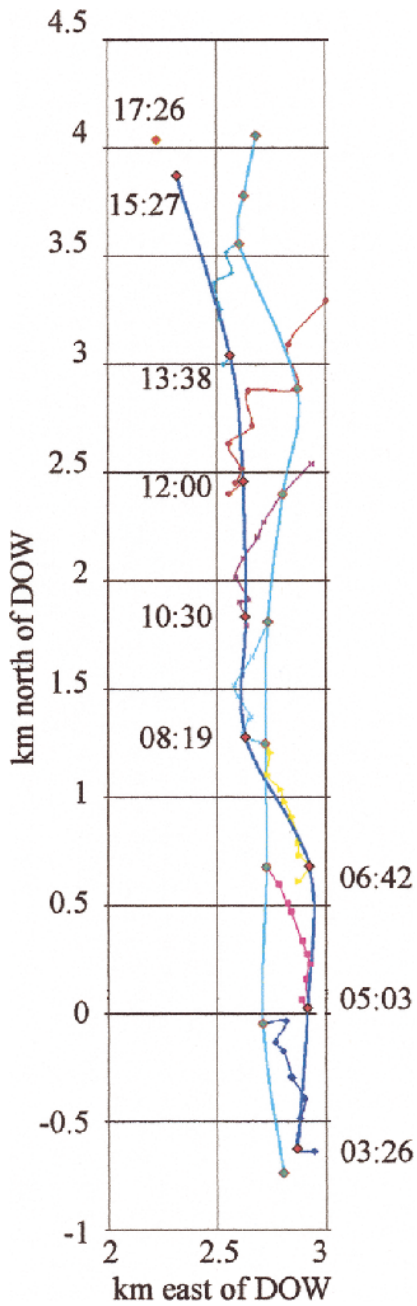
FIG. 17. Track of tornado near the ground and at 1 km AGL. The low-level track (dark blue) exhibited a deviation toward the northwest, while the path at 1 km AGL (light blue) remained very constantly northward. Short wavy line segments connect the location of the tornado center in each radar scan and help illustrate the westward inclination of the tornado in the early observations and the eastward inclination later. Numerals are times, mm:ss after 0100 UTC, of the lowest-level radar scans.
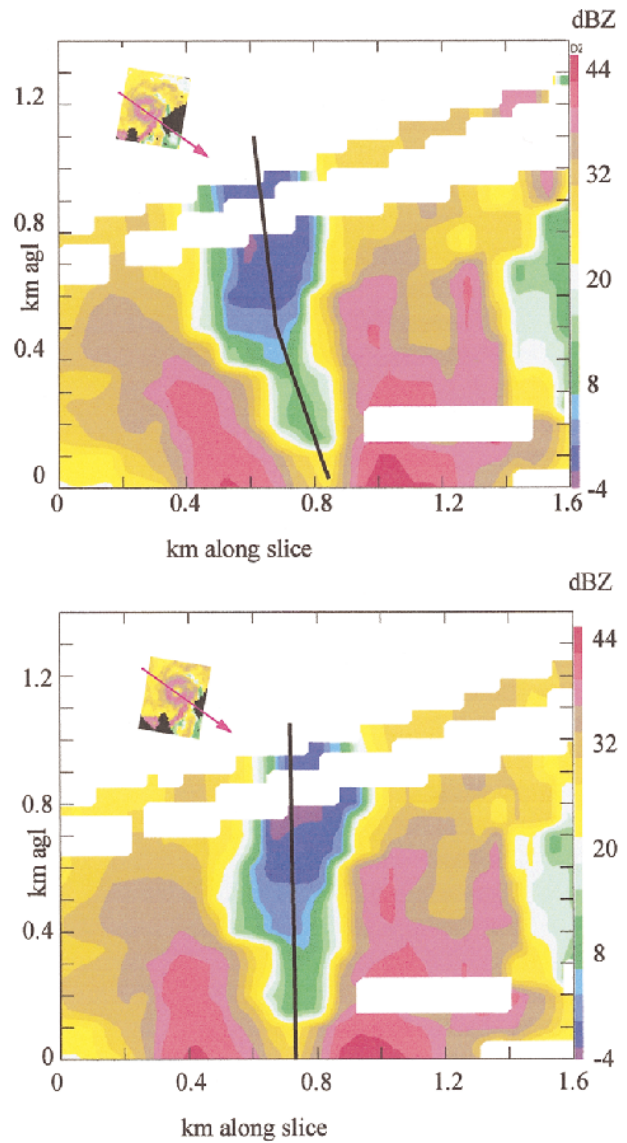

FIG. 18. Vertical cross sections through the reflectivity field of the tornado indicating (left) true tilt and (right) artificial vertical stacking used for analysis. The plotted slices extended approximately along the axis of inclination and through the center of the debris ring as indicated in the insets (where north was up). The inclination of the debris cloud was approximately 20° below 400 m AGL and 10° above up to 1 km AGL as indicated by the broken black line. Plotted aspect ratio is nearly 1:1.

radius was too small, ~300 m, to be well resolved by the current observations. Rankine profiles were matched to all 75 observed profiles. Figure 21 illustrates a typical profile with a corresponding Rankine curve forced to match the observed core radius and peak wind speed.

The matches in almost all cases indicated that the observed winds decayed more slowly than R^{-1}. Sources of observational error included errors in tornado motion corrections (± 1.5 m s^{-1}). When a simple $V \sim R^{\alpha}$ curve fit was applied, likely errors in tornado motion calculations accounted for a ± 0.05 error in α. Burgess et al. (1993) used the aspect ratio, or ratio of radar beamwidth to tornado core radius, R_0 to evaluate radar sampling of vortices. The aspect ratio for the DOW observations in Dimmitt was 0.5–0.8, indicating that peak wind speeds

might have been underestimated by as much as 10%–20% compared to Rankine vortex predictions.

Comparison of the DOW observations with more realistic model vortex structures (Houze 1993) would probably result in closer agreement since these more realistic models do not contain the sharp Rankine peak velocity at R_0. Unfortunately, as discussed above, the current observations do not contain enough information to define such vortices. When simple exponential decay curves ($V \sim R^\alpha$) were matched to the outer flow ($R > R_0$) region, α ranged from 0.5 to 0.7. Interestingly, this is typical of the wind field decay rates observed in hurricanes. It implies that the angular momentum in the tornado was not constant with radius, but decays toward the center.

g. Comparison of radar wind measurements with Fujita-scale rating

Peak DOW-measured raw Doppler velocities were 74 m s^{-1} at 0102:54 UTC near 600 m AGL and at 0105:32 UTC near 200 m AGL. With adjustments for observation aspect ratio [approximating relevant portion of the curve presented in Burgess et al. (1993)] with a linear relation, $V_{adj} = V_{Doppler}[1 - 0.24(B/r)]^{-1}$, where B is the radar beamwidth and r is the core radius, and correcting for tornado motion, the peak vortex relative wind speed was 89 m s^{-1} and the peak ground relative velocity was 95 m s^{-1}. The aspect ratio corrections were particularly sensitive to subjectivities in the dealiasing of the core region of the tornado and were likely subject to errors of at least 10% or ± 7 m s^{-1}. Futhermore, they assume that the wind field structure near R_0 approximated that predicted by the Rankine model. Turbulent diffusion near R_0 would likely reduce the magnitude of the maximum tangential velocity, so the above estimates of peak velocity probably overestimate true values by several meters per second. One of the authors (JW) observed that the tornado had removed a 40-m length of asphalt from Highway 86 and found severe damage to a house and cars that had been lofted and dragged from near the highway (Fig. 22). VORTEX survey teams estimated this and other damage in this area equivalent to a Fujita-scale rating of F4 (estimated wind speeds >92.5 m s^{-1}) (http://doplight.nssl.noaa.gov/projects/vortex/events/damage/dimmittTrackTimes.gif). The official damage intensity rating reported in NOAA (1995) is F2. DOW measurements indicated aspect-ratio-adjusted ground-relative wind speeds of 82 m s^{-1} near that location (Table 1; Fig. 2). This is at least 10 m s^{-1} lower than the F4 rating assigned by VORTEX damage surveys and is similarly higher than the official estimates based on F2 damage, but still represents remarkably close agreement given the uncertainties associated with the damage survey and the Doppler measurements.

With the advent of mobile Doppler radars such as the DOWs, it is often possible to obtain direct high-resolution wind measurements inside tornadoes. Since Fu-jita-scale ratings are dependent on the availability and strength of structures, it is useful to introduce a *potential Fujita* (PF) scale based on direct wind observations. The PF scale characterizes the Fujita-scale-equivalent damage that a tornado could potentially cause, if it passed through a developed region. A PF rating is defined as, the Fujita-scale damage intensity that would result *if* the tornado passed over a region with strength-classifiable structures, assuming the wind speed calibration of the F scale is correct and the radar is fully resolving the winds. An observer could meaningfully say of a PF3 rated tornado that, "This tornado contains winds that could potentially cause F3 level damage if it passed through a town (though it might be only causing F0 damage in a field at this moment)." The use of this scale to rate tornadoes in which wind speeds are directly measured (or even inferred) could reduce significantly the popular confusion associated with the discrepancies between measured winds (often extremely high), and the minor damage that occurs in most tornadoes due to the dearth of structures affected.

As high-resolution mobile radars produce observations at smaller and smaller scales, it will be necessary to refine the methods of comparison between radar wind measurements and structural damage to account for the short timescales associated with very small radar resolution volumes. For example, consider a 100 m s^{-1} wind observed in a single 10-m-scale radar resolution volume. A stationary structure may be impacted by this extreme wind speed for only 0.1 s. Wind gusts that last for such short times may or may not cause significant damage. Extremely high resolution radar measurements of mean Doppler velocity, and particularly extremes of radar spectral measurements of Doppler velocity, which may be associated with very small spatial scales or even single airborne objects, should only be compared with anemometer-based wind measurements after careful consideration of the respective timescales.

The peak PF rating in the Dimmitt tornado, including aspect ratio corrections (Burgess et al. 1993) was PF4, as the tornado crossed Highway 194 after 0105 UTC, with PF3 indicated through 0112 UTC after the tornado crossed Highway 86. As discussed before, peak DOW aspect-ratio-adjusted ground-relative wind speeds were 95 m s^{-1} at 0105 UTC.

h. Convergence

Conceptual and computer models of tornadoes have predicted that there should be strong convergence near the surface in a tornado. Lewellen et al. (1997) predicted that strong inward radial flow, approximately 50 m s^{-1}, should occur below 30 m AGL. This would be almost impossible to observe with conventional or airborne radars (Wurman et al. 1997). In fact, the nonobservation of strong surface convergence, and the resultant error in the boundary condition for vertical integration of the continuity equation, might have accounted for the re-
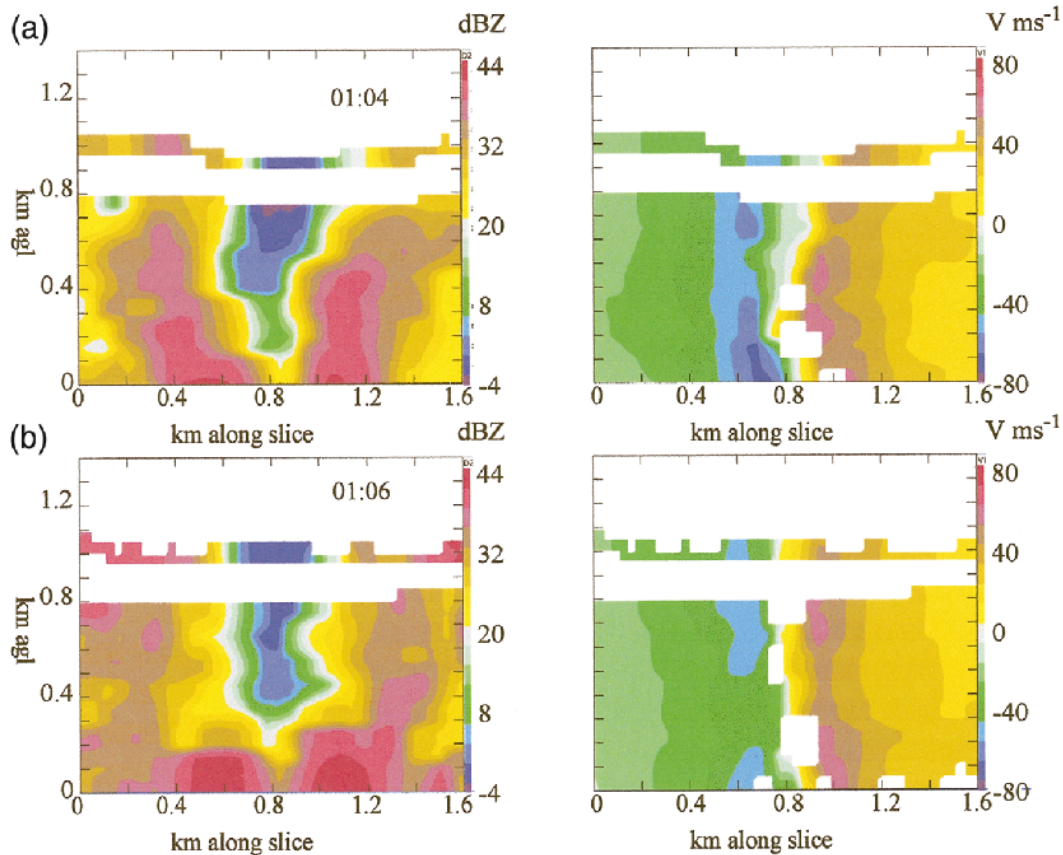
FIG. 19. Vertical cross sections through tornado reflectivity and Doppler velocity fields at 0104, 0106, 0108, and 0110 UTC. Prominent debris clouds can be seen extending from the ground to above 800 m AGL at 0104 UTC. But the altitude to which they extended decreased to only 200–400 m AGL by 0110 UTC. Strong winds near the surface in excess of 65 m s^{-1} weakened slightly with height at 0104 UTC. Weaker winds (partially due to choice of cross

ported downdraft in the dual-Doppler analysis of Wakimoto and Martner (1992). This lower boundary condition is particularly difficult to characterize in the region of a tornado where vertical motions just above the surface may be large. Since the DOW was capable of collecting data in the <100 m AGL layer, it was hoped to measure the magnitude of the convergence into the tornado. The Doppler velocity couplets in Fig. 7 would have been rotated significantly if convergent wind speeds of even 10 m s^{-1} were present. However, this was not observed and the Doppler velocity signatures were characteristic of almost purely vortical flow. Even at the lowest observed levels, 30 m AGL, when the tornado was <3 km from the DOW, convergence was not evident (Fig. 23) near the tornado center. However convergence was indicated at distances over about 400 m from the tornado center in some observations, notably at 0105:03 UTC to the north of the tornado (inbound or negative velocity side). The velocity maximum at distances of 400–1000 m from the tornado center appears to be rotated by approximately 15°. This implies that velocities into the tornado of up to 10 m s^{-1} may have been present. It is tempting to calculate the implied

convergence; however, the absence of a similar rotation of the Doppler velocity maxima on the southern side (outbound or positive velocity side) makes this calculation problematical. In the tornado itself, convergence was either not present, or more likely, was present but not observed. There were two possible causes for the inability to observe the convergence. It was possible that the convergence was confined to a region below the peak intensity of the lowest radar beams, or below 30 m AGL. It was more likely that centripetal accelerations affecting the debris masked any convergence that was present in the air velocity field. A simple formulation existed (D. Dowell 1999, personal communication) for calculating the magnitude of the convergence that may be masked. The tornado wind field could be idealized as $V_r = -\delta R/2$ and $V_\theta = \zeta R/2$, where V_r is the radial velocity and V_θ is the tangential velocity, and R is the radial distance from the center of the tornado, ζ is the relative vertical vorticity, and δ is the convergence. It could be further assumed that the particles in the main debris cloud circled the vortex while maintaining a balance between centripetal acceleration and drag, that is, circling the tornado at relatively con-
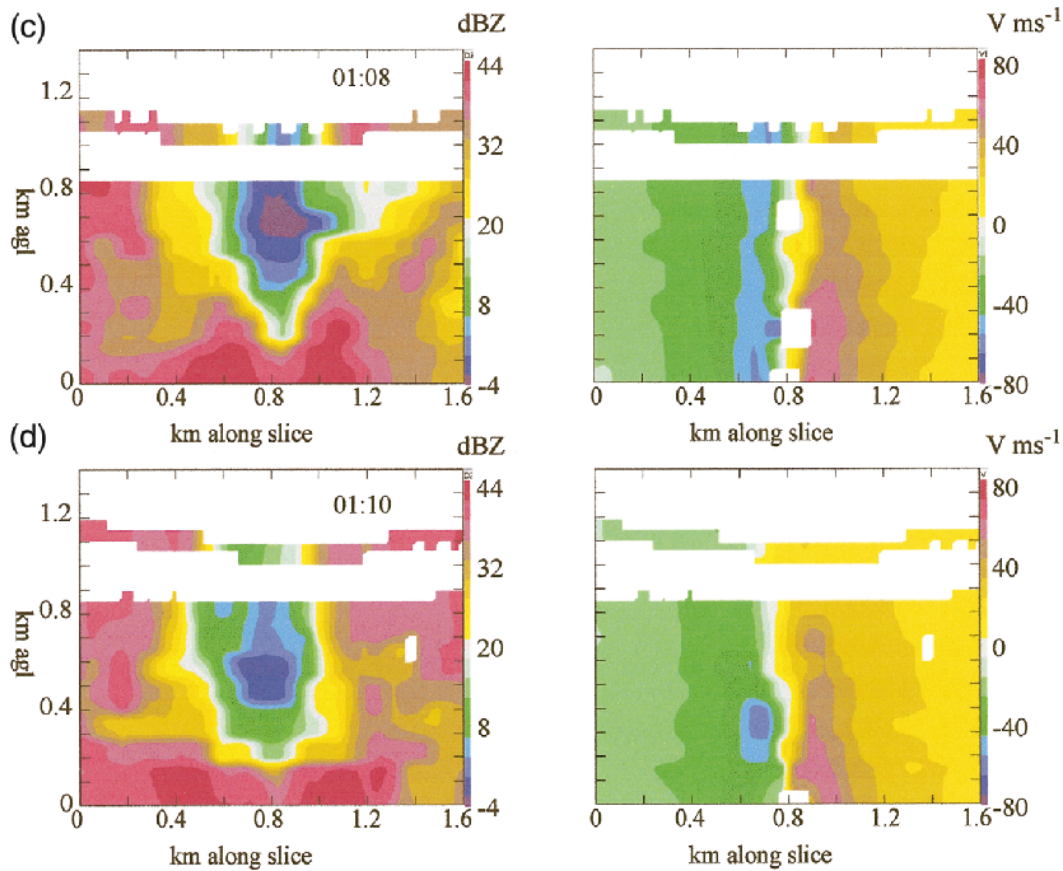
FIG. 19. (*Continued* section) weakened sharply above 600 m AGL by 0110 UTC. The start of the rapid decrease in volumetric extent of winds >40 m s^{-1} can be seen at 0110 UTC. Velocity is in m s^{-1}. Reflectivity is in uncalibrated dBZ. Plotted aspect ratio is 1:1. Cross-section orientation is nearly perpendicular to DOW beams in order to capture maximum Doppler velocity.
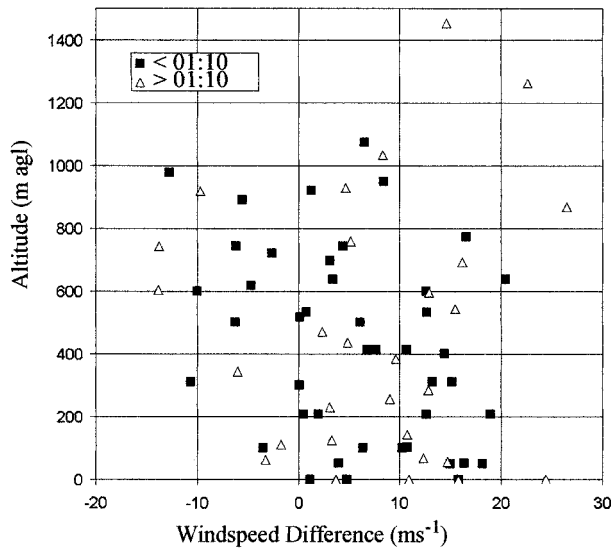

FIG. 20. Difference between magnitude of away and toward *vortex-relative* peak wind speeds in tornado not adjusted for aspect ratio. Stronger winds on the eastern (away) side of the tornado are evident in most scans.

stant radius. Following Rogers and Yau (1989), the drag force on the, assumed, spherical particles was $F_{\mathrm{drag}} = (\pi/2)r^2V_r^2\rho_aC_d$, where r is the radius of the particle, ρ_a is the air density, and C_d is the drag coefficient. The mass of the particle was given by $m = (4/3)\pi r^3\rho_s$, where ρ_s was the density of the particles. These could be solved for δ resulting in $\delta^2 = (8\rho_s\zeta^2 r)/(3R\rho_aC_d)$. White (1991) provided C_d for smooth spheres ranging from $C_d = 0.5$ for a 2-mm diameter sphere to $C_d = 0.1$ for a 1-m diameter sphere. In the absence of vector wind observations, ζ could be approximated as twice the azimuthal shear, resulting in values near 1.0 s^{-1} (using shear = 0.5 s^{-1} from Fig. 11). Table 2 illustrates the values of convergence that might have been masked under differing assumptions concerning the nature of the debris scatterers responsible for most of the energy return to the radar. Values for large objects such as chickens and small cows should be regarded with some skepticism. A final possibility is that the convergence was confined to an extremely narrow region below the lowest observation levels ($\sim$30 m AGL). Strong convergence toward the tornado was observed visually, but it was impossible to determine vertical extent. Preliminary analysis of

more recent low-level DOW observations of tornadoes, some from as low as 10 m AGL, did not reveal convergence.

The absence of observed convergence inside the debris ring, and the occasional observation of strong convergence just outside the ring, is consistent with the analysis presented above. Strong divergence was not observed at any level.

i. Turbulence and suction vortices

Since it was likely that subtornado-scale features such as suction vortices were too small to resolve directly, spectral width data were examined in the hope that such features would result in isolated regions of enhanced values. Anomalously high spectral width regions were observed and may have been associated with suction vortex–like features. However, they did not maintain any observable temporal or spatial continuity from scan to scan. It was likely that any such features had lifetimes shorter than the inter–volume scan interval of 100 s. Even if persistent, they would probably have rotated significantly around the central vortex from single elevation scan to scan (10 s) and would thus have been almost impossible to discern. A vertically oriented object located at a distance of 200 m from the center of the tornado, moving at 60 m s^{-1}, would travel 600 m between scans, circumscribing an arc of nearly 180°, appearing on alternate sides of the tornado in each subsequent scan. Much faster radar observations would have been required to characterize such features. Even with more rapid radar updates, the three-dimensional reconstruction of such objects would have been difficult. A reconstruction correcting only for bulk tornado motion would have resulted in vertical suction vortices being perturbed into helixes. Correct reconstruction would have required ''dehelixizing'' these structures using nonlinear time–space corrections.

When the tornado exhibited a strong downdraft during the earliest observation times, a ring of high spectral width surrounded the downdraft region (Fig. 24). This might have been due to particularly turbulent flow in the strong shear region between the central downdraft and the spiraling upward flow. The downdraft region was characterized by relatively low spectral width, implying less turbulence.

4. Conclusions

The unprecedented high-resolution radar observations of the Dimmitt, Texas (3 June 1995), tornado presented herein have revealed new structures and confirmed the existence of modeled and theorized structures, including a central downdraft. They illustrated that peak wind speed might not have been the best measure of total tornado strength, or at least that it may mask significant weakening of the bulk circulation both horizontally at the surface and aloft. Volumetric mea-
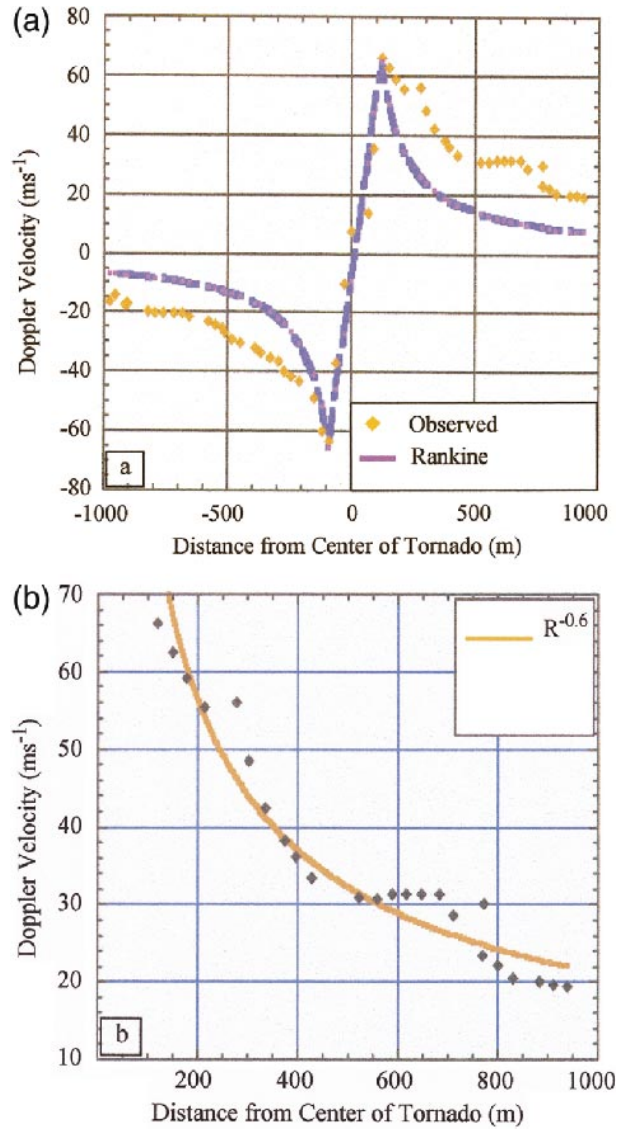

FIG. 21. Distribution of Doppler velocities vs distance from center of tornado. (b) Winds on either side of tornado did not appear to exhibit R^{-1} dependence as predicted by conservation of angular momentum during inflow. Winds in the core region might have been underestimated due to observation aspect ratio limitations, but the general trend in this profile and most others was $V \sim R^{-0.6}$. Best exponential fit for innermost 1000 m of tornado for this profile is shown in (b).

sures of tornado strength such as the volume affected by certain threshold winds were found to be illuminating. Evidence of nonangular momentum conserving flow in the form of slowly decreasing winds with distance from the tornado center may be in conflict with some computer and conceptual models. These data provided the first direct, if crude, comparisons of actual high-resolution radar wind measurements with the Fujita damage rating scale. While these data were revealing, higher resolution, both spatially and temporally, and dual-Doppler radar observations, currently in prelimi-
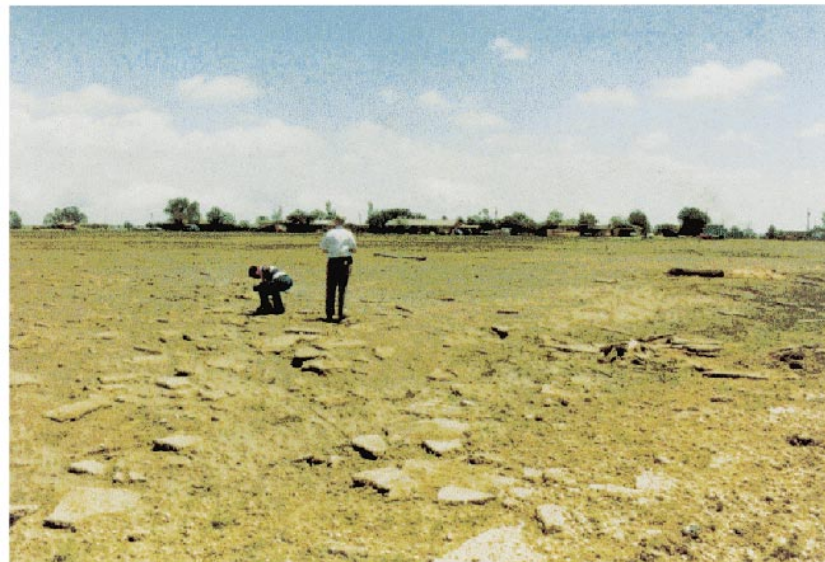
FIG. 22. Damage caused by tornado north of Highway 86. (a) Car lofted and dragged from near highway. Another car, lofted and dragged several hundred meters, is visible in the distance near the horizon near the left edge of the photograph. Direction of photograph is approximately northward. (b) Scoured farm field with pieces of asphalt removed from the highway. Photograph was taken toward the northeast with the eastern edge of the damage path visible in the background. Both photographs were taken the day after the tornado at approximately 1600–1700 UTC 3 Jun 1995.

nary analysis and being attempted, offer the promise of more quantitative analyses of many of the structures described in this work and the better characterization of the rapid evolution of the torando.[1]

TABLE 2. Convergence (s^{-1}) possibly missed in radar observations of various types of debris.

Object	Diameter (m)	Density (kg m^{-3})	Drag coefficient	Masked convergence (s^{-1})
Raindrop	0.002	1000	0.5	0.3
Gravel	0.02	3000	0.5	1.6
Brick	0.1	2000	0.3	3.8
Chicken/cow	1	1000	0.1	8

[1] Processed and raw DOW radar data from the Dimmitt tornado and other tornadoes observed in 1995 are available via anonymous ftp from the University of Oklahoma. Information concerning the downloading and interpretation of the data can be found at http://aaron.ou.edu/data_availability.html.
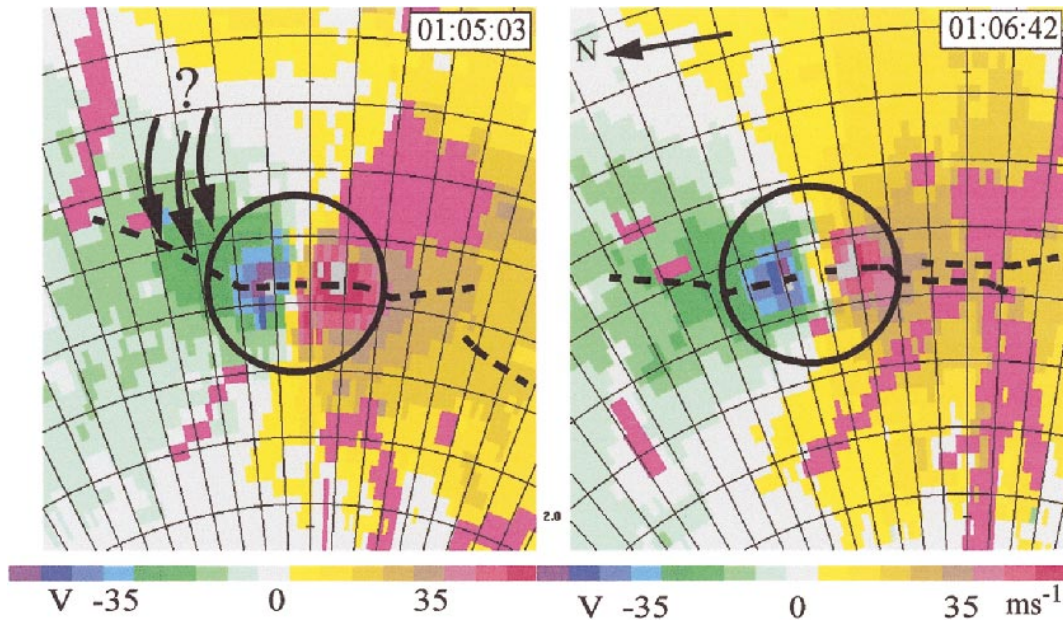
FIG. 23. Lowest elevation velocity data showing lack of measured convergence. Lowest elevation scans, 0°, in second and third volumetric samples at (left) 0105:03 UTC and (right) 0106:42 UTC (data from 0103:26 UTC were too contaminated by ground clutter) reveal strong velocity couplets and severe ground clutter contamination, but little convergence inside debris rings (black circles). Positive (away) and negative (toward) high velocity regions were oriented nearly tangentially to radar beams (angle <10°), indicating unmeasurable convergent velocities of <10 m s^{-1}. The subjectively determined axes of maximum Doppler velocity are indicated by the dashed black lines. Outside debris rings, there is some evidence of convergence on the north side (inbound, green) side of the tornado where the maxima are rotated by ~15°. Rotation of the velocity maxima in those regions suggests inbound velocities as high as 10 m s^{-1}. *Range rings are spaced at 300-m intervals.* Velocities are in m s^{-1}. The direction of the DOW can be seen by the converging radial grid lines. Pink/lavender regions contain data excluded due to clutter or noise.
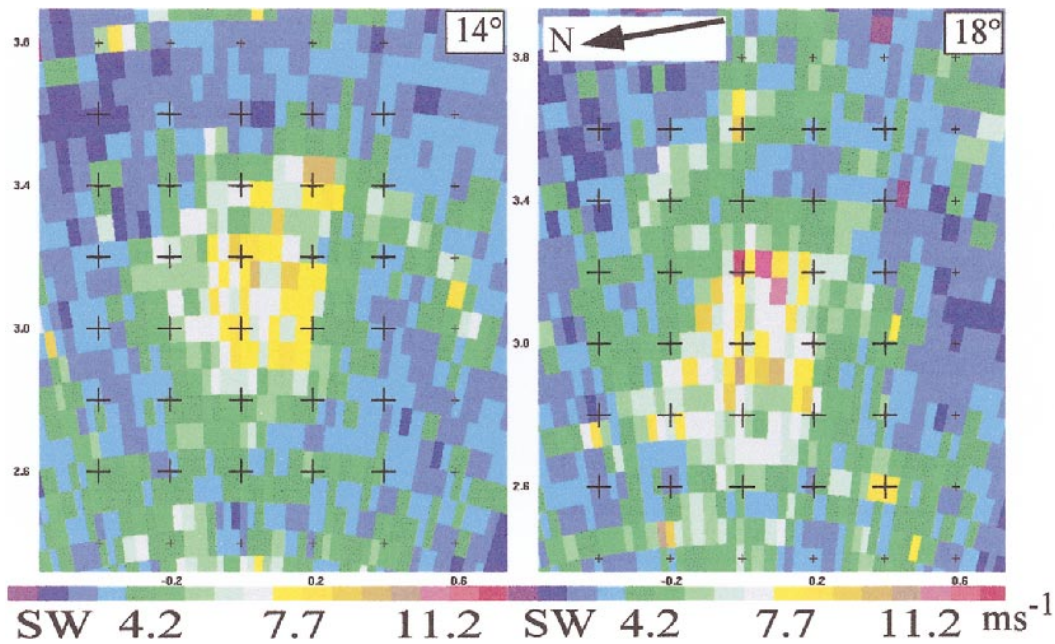

FIG. 24. Spectral width of velocity data in the downdraft region. A ring of high spectral width surrounded the central downdraft in the highest elevation data, (left) 14° and (right) 18°, near 1 km AGL taken between 0104:41 and 0105:0000 UTC. Airflow in the downdraft was relatively nonturbulent compared to that at the core radius of the tornado. Spectral width values are in m s^{-1}. *Tick marks define a grid with 200-m spacing.*

REFERENCES

Bluestein, H. B., J. G. LaDue, H. Stein, D. Spegher, and W. P. Unruh, 1993: Doppler radar wind spectra of supercell tornadoes. *Mon. Wea. Rev.,* **121,** 2200–2221.

——, A. L Pazmany, J. C. Galloway, and R. E. McIntosh, 1995: Studies of the substructure of severe convective storms using a 3-mm wavelength Doppler radar. *Bull. Amer. Meteor. Soc.,* **76,** 2155–2169.

Brandes, E. A., 1984: Vertical vorticity generation and mesocyclone sustenance in tornadic thunderstorms: The observational evidence. *Mon. Wea. Rev.,* **112,** 2253–2269.

Brown, R. A., L. R. Lemon, and D. W. Burgess, 1978: Tornado detection by pulsed Doppler radar. *Mon. Wea. Rev.,* **106,** 29–38.

Burgers, J. M., 1948: A mathematical model illustrating the theory of turbulence. *Advances in Applied Mechanics,* R. von Mises and T. von Karman, Eds., Academic Press, 171–199.

Burgess, D. W., and L. R. Lemon, 1990: Severe thunderstorm detection by radar. *Radar in Meteorology,* D. Atlas, Ed., Amer. Meteor. Soc., 619–647.

——, R. J. Donaldson Jr., and P. R. Desrochers, 1993: Tornado detection and warning by radar. *The Tornado: Its Structure, Dynamics, Prediction and Hazards, Geophys. Monogr.,* No. 79, Amer. Geophys Union, 203–221.

Carbone, R. E., M. J. Carpenter, and C. D. Burghart, 1985: Doppler radar sampling. *J. Atmos. Oceanic Technol.,* **2,** 357–361.

Church, C. R., and J. T. Snow, 1993: Laboratory models of tornadoes. *The Tornado: Its Structure, Dynamics, Prediction and Hazards, Geophys. Monogr.,* No. 79, Amer. Geophys Union, 19–39.

——, G. L. Baker, and E. M. Agee, 1979: Characteristics of tornado-like vortices as a function of swirl ratio: A laboratory investigation. *J. Atmos. Sci.,* **36,** 1755–1776.

Davies-Jones, R. P., 1973: The dependence of core radius on swirl ratio in a tornado simulator. *J. Atmos Sci.,* **30,** 1427–1430.

——, 1986: Tornado dynamics. *Thunderstorm Morphology and Dynamics,* 2d ed., E. Kessler, Ed., University of Oklahoma Press, 197–236.

Doviak, R. J., and D. S. Zrnic, 1993: *Doppler Radar and Weather Observations.* Academic Press, 562 pp.

Fiedler, B. H., and R. Rotunno, 1986: A theory for the maximum windspeeds in tornado-like vortices. *J. Atmos. Sci.,* **43,** 2328–2340.

Fujita, T., 1958: Mesoanalysis of the Illinois tornadoes of 9 April 1953. *J. Meteor.,* **15,** 288–296.

——, 1970: The Lubbock, Texas tornadoes: A study of suction spots. *Weatherwise,* **23,** 160–173.

Hildebrand, P. H., and C. K. Mueller, 1985: Evaluation of meteorological airborne Doppler radar. Part I: Dual-Doppler analyses of air motions. *J. Atmos. Oceanic Technol.,* **2,** 362–380.

Houze, R., 1993: *Cloud Dynamics.* Academic Press, 573 pp.

Johnson, K. W., P. S. Ray, B. C. Johnson, and R. P. Davies-Jones, 1987: Observations related to the rotational dynamics of the 20 May 1997 tornadic storms. *Mon. Wea. Rev.,* **115,** 2463–2478.

Keeler, J. R., B. W. Lewis, and G. R. Gray, 1989: Description of NCAR/FOF CP-2 meteorological Doppler radar. Preprints, *24th Conf. on Radar Meteorology,* Tallahassee, FL, Amer. Meteor. Soc., 589–592.

Lawrence, M. B., and B. M. Mayfield, 1977: Satellite observations of trochoidal motion of Hurricane Bell 1976. *Mon. Wea. Rev.,* **105,** 1458–1461.

Levison, C. H., 1997: Long-range transport of debris by tornadic thunderstorms: A multi-case perspective, M.S. thesis, School of Meteorology, University of Oklahoma, 189 pp. [Available from School of Meteorology, University of Oklahoma, Norman, OK 73019.]

Lewellen, W. S., 1993: Tornado vortex theory. *The Tornado: Its Structure, Dynamics, Prediction and Hazards, Geophys. Monogr.,* No. 79, Amer. Geophys. Union, 19–39.

——, D. C. Lewellen, and R. I. Sykes, 1997: Large-eddy simulation of a tornado's interaction with the surface. *J. Atmos. Sci.,* **54,** 581–605.

NOAA, 1995: *Storm Data.* Vol. 37, No. 6, 224 pp.

Rasmussen, E. N., and C. Crosbie, 1995: Tornado damage assessment in VORTEX-95. Preprints, *18th Conf. on Severe Local Storms,* San Francisco, CA, Amer. Meteor. Soc., 153–157.

——, J. M. Straka, R. Davies-Jones, C. A. Doswell III, F. H. Carr, M. D. Eilts, and D. R. MacGorman, 1994: Verification of the Origin of Rotation in Tornadoes Experiment: VORTEX. *Bull. Amer. Meteor. Soc.,* **75,** 995–1006

Rogers, R. R., and M. K. Yau, 1989: Initiation of rain in non-freezing clouds. *A Short Course In Cloud Physics,* 3d ed., D. T. Haar, Ed., Pergamon Press, 121–149.

Rott, N., 1959: On the viscous core of a line vortex. *J. Appl. Math. Phys.,* **9b,** 543–553.

Rotunno, R., 1977: Numerical simulation of a laboratory vortex. *J. Atmos. Sci.,* **34,** 1942–1956.

——, 1979: A study of tornado-like vortex dynamics. *J. Atmos. Sci.,* **36,** 140–154.

——, 1984: An investigation of a three-dimensional asymmetric vortex. *J. Atmos. Sci.,* **41,** 283–298.

——, 1986: Tornadoes and tornadogenesis. *Mesoscale Meteorology and Forecasting,* P. S. Ray, Ed., Amer. Meteor. Soc., 414–436.

Smith, R. L., and D. W. Holmes, 1961: Use of a Doppler radar in meteorological observations. *Mon. Wea. Rev.,* **89,** 1–7.

Wakimoto, R. M., and B. E. Martner, 1992: Observations of a Colorado tornado. Part II: Combined photogrammetric and Doppler radar analysis. *Mon. Wea. Rev.,* **120,** 520–543.

——, and N. T. Atkins, 1996: Observations on the origins of rotation: The Newcastle tornado during VORTEX-94. *Mon. Wea. Rev.,* **124,** 384–407.

——, W.-C. Lee, H. B. Bluestein, C.-H. Liu, and P. H. Hildebrand, 1996: ELDORA observations during VORTEX-95. *Bull. Amer. Meteor. Soc.,* **77,** 1465–1481.

——, C. Liu, and H. Cai, 1998: The Garden City, Kansas, storm during VORTEX 95. *Mon. Wea. Rev.,* **126,** 372–408.

Ward, N. B., 1972: The exploration of certain features of tornado dynamics using a laboratory model. *J. Atmos. Sci.,* **29,** 1194–1204.

White, F. M., 1991: Solutions of the Newtonian viscous flow equations. *Viscous Fluid Flow,* 2d ed., L. Beamsderfer and J. M. Morriss, Eds., McGraw-Hill, 105–217.

Willoughby, H. E., and M. B. Chelmow, 1982: Objective determi-

nation of hurricane tracks from aircraft observation. *Mon. Wea. Rev.,* **110,** 1298–1305.

Wood, V. T., and R. A. Brown, 1997: Effects of radar sampling on single-Doppler velocity signatures of mesocyclones and tornadoes. *Wea. Forecasting,* **12,** 928–938.

Wurman, J., J. M. Straka, and E. N. Rasmussen, 1996: Fine-scale Doppler radar observations of tornadoes. *Science,* **272,** 1774–1777.

——, ——, ——, M. Randall, and A. Zahrai, 1997: Design and deployment of a portable, pencil-beam, pulsed, 3-cm Doppler radar. *J. Atmos. Oceanic Technol.,* **14,** 1502–1512.

Zrnic, D. S., and R. J. Doviak, 1975: Velocity spectra of vortices scanned with a pulse-Doppler radar. *J. Appl. Meteor.,* **14,** 1531–1539.

——, D. W. Burgess, and L. Hennington, 1985: Doppler spectra and estimated windspeed of a violent tornado. *J. Climate Appl. Meteor.,* **24,** 1068–1081.